IONOSPHERIC IRREGULARITIES: ALASKA PHOTOMETRIC MEASUREMENTS

Robert D. Sears

Lockheed Missiles and Space Company

Prepared for:

Defense Nuclear Agency

4 December 1973

Destroy this report when it is no longer needed. Do not return to sender.

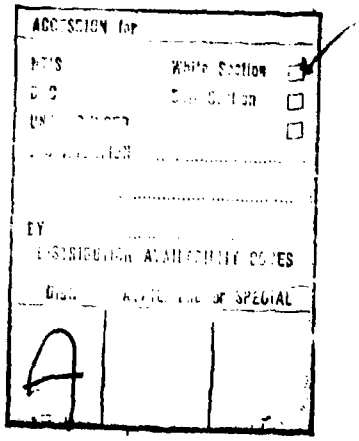

Field Command Printing Division

UNCLASSIFIED

SECURITY CLASSIFICATION OF THIS PAGE (When Data Entered)

AD 776 241

REPORT DOCUMENTATION PAGE

READ INSTRUCTIONS BEFORE COMPLETING FORM

1. REPORT NUMBER: DNA 3235F	2. GOVT ACCESSION NO.
3. RECIPIENT'S CATALOG NUMBER	
4. TITLE (and Subtitle): IONOSPHERIC IRREGULARITIES: ALASKA PHOTOMETRIC MEASUREMENTS	5. TYPE OF REPORT & PERIOD COVERED: Final Report for Period 1 Dec 72 - 30 Nov 73
	6. PERFORMING ORG. REPORT NUMBER: LMSC D354546
7. AUTHOR(s): Robert D. Sears	8. CONTRACT OR GRANT NUMBER(s): DNA 001-73-C-0110
9. PERFORMING ORGANIZATION NAME AND ADDRESS: Lockheed Palo Alto Research Laboratory, 3251 Hanover Street, Palo Alto, California 94304	10. PROGRAM ELEMENT, PROJECT, TASK AREA & WORK UNIT NUMBERS: NWET SUBTASK K43AAXHX615-03.
11. CONTROLLING OFFICE NAME AND ADDRESS: Director, Defense Nuclear Agency, Washington, D.C. 20305	12. REPORT DATE: 4 December 1973
	13. NUMBER OF PAGES: 80
14. MONITORING AGENCY NAME & ADDRESS(if different from Controlling Office)	15. SECURITY CLASS. (of this report): UNCLASSIFIED
	15a. DECLASSIFICATION/DOWNGRADING SCHEDULE

16. DISTRIBUTION STATEMENT (of this Report)

Approved for public release; distribution unlimited.

17. DISTRIBUTION STATEMENT (of the abstract entered in Block 20, if different from Report)

18. SUPPLEMENTARY NOTES

19. KEY WORDS (Continue on reverse side if necessary and identify by block number)

Photometer
Auroral Emissions
4278 Å 6300 Å
5577 Å 5875 Å
Ionospheric Irregularities
Particle Precipitation
Energy Deposit

20. ABSTRACT (Continue on reverse side if necessary and identify by block number)

Photometric measurements of auroral intensities and structure were made in Alaska during 1972 and 1973. Photometric data supporting the ICE CAP '73A operations are presented in terms of definition of the energy input to the ionosphere in the spatial vicinity of the rocket borne in situ experiments. Coordinated analysis of spatial and temporal variations of auroral emission intensities and electron densities are outlined utilizing both photometric intensity data and incoherent scatter radar data. Analysis of time variations

DD FORM 1 JAN 73 1473 EDITION OF 1 NOV 65 IS OBSOLETE

UNCLASSIFIED

SECURITY CLASSIFICATION OF THIS PAGE (When Data Entered)

20. ABSTRACT (Continued).

of 4278Å, 5875Å, and 4861Å emission intensities observed in 1972 indicates strong substorm time correlation with the intensity peaks, but no indication of He emission in the 5875Å spectral region was found. An analytical method for converting F region 6300Å, OI emission intensity structure maps into radar effects structure information was demonstrated for a low latitude region pertinent to radar scintillation effects measurements at Kwajalein Missile Range.

PREFACE

This is the final report on Contract DNA 001-73-C-0110, entitled "Measurement of Ionospheric Irregularities." The period of work was from 1 December 1972 through 30 November 1973. This program is a continuation of previous research efforts under similar titles which have involved development and utilization of photometric methods for measurements of ionospheric radiance irregularities which may characterize structured ionization features, structured infrared emission features, or existence of spatially non-uniform features in energy deposition by a variety of physical processes.

The principal investigator on this program wishes to acknowledge the efforts and support of the following personnel: Messrs. D. Hillendahl and A. Fernandez of LMSC who provided invaluable technical and computer programming support, Dr. J.E. Evans and B.M. McCormac who provided valuable support and advice on the program, and Dr. C.A. Blank and Lt. H. Mitchell, our technical contacts at DNA. Several Stanford Research Institute personnel provided valuable assistance at the Chatanika field site, in particular, Messrs. J. Briski and J. Hodges. Coordinated experiments with SRI at Chatanika were greatly facilitated through cooperation of Drs. M. Baron, W. Chesnut, C. Rino and V. Wickwar.

TABLE OF CONTENTS

		Page
PREFACE		1
I.	INTRODUCTION	3
II.	EXPERIMENTAL RESULTS	5
	A. Operational Summary	6
	B. ICE CAP Energy Input Data	9
III.	ANALYTICAL RESULTS	19
	A. Coordinated Radar-Photometer Experiment on O(^{1}S) Excitation and Deionization Chemistry	19
	B. Analytical Prediction of Expected Radar Degradation at Kwajalein Missile Range from Observed F-Region Optical Structure	28
	C. Observations of Substorm Time Variations in 4278Å, 4861Å and 5875Å Emissions During the ICE CAP 1972 Experiment	36
IV.	CONCLUSIONS AND RECOMMENDED FUTURE WORK	53
REFERENCES		55
APPENDIX 1		57
APPENDIX 2		78

I. INTRODUCTION

"Measurement of Ionospheric Irregularities" is a continuation of a program begun several years ago under the auspices of the high altitude nuclear test readiness program. The goal of this program was and continues to be: development and application of a capability for obtaining photometric measurements of irregularities in ionospheric radiance which may be interpreted in terms of spatial and temporal structure of ionized irregularities, infrared emission irregularities, and/or irregularities in energy deposited in the upper atmosphere by a variety of natural or artificial processes. Optical measurements made during this program were coordinated with other experiments including ionospheric sounders, incoherent scatter and clutter radars, and rocket and ground-based infrared measurements.

Development and test of photometric instrumentation for ionospheric radiance irregularity measurements was reported in DNA 2997T (reference 1). Use of the new instrumentation at Goose Bay, Labrador as part of a coordinated ionospheric research program, and in Alaska as part of an infrared emission measurements program (ICE CAP '72) was reported in references 2 and 3 respectively (DNA 2985F and DNA 3033F). In this report we summarize certain analytical results obtained subsequent to the date of reference 3 as well as the results of experimental operations conducted at Chatanika, Alaska in the spring of 1973.

During the period of the subject contract, the following experimental and analytical areas were studied: photometric measurements of energy input at the Chatanika, Alaska field site from charged particle precipitation were made in coordination with ICE CAP '73 rocket experiments and also in close cooperation with the SRI/DNA incoherent scatter radar; photometric measurements to attempt to detect and describe the transport of energy and excited species in the auroral ionosphere were made simultaneously with the energy input measurements; continued development of analytical methods for processing the photometric data and interpreting it in terms of energy input and transport was undertaken; and an analytical

demonstration of the cbility to predict radar scintillation effects of F-region irregularities, given a photometric irregularity map of F-region emissions was completed. Experimental measurements were made with the previously described trichroic filter photometer and with the 3-beam photometer. Operation of these photometers was simultaneous with a data interval typically of 1 second. About 120 hours of such data were obtained from three separate trips to the Chatanika field site, of w'c:, about 100 hours or so was of useful quality and was computer processed to an editing format. About half of this data was obtained as direct support to the ICE CAP '73 rocket experiments. The remainder of the time on site was spent in operating coordinated radar-optical experiments in cooperation with SRI and University of Alaska personnel. These latter experiments were oriented mainly towards detection and description of ionospheric wavelike and/or turbulent disturbances, and to obtaining statistical time series emission intensity data from which ionospheric recombination coefficients could be derived.

Because it has become increasingly clear during the progress of the DNA High Altitude Effects Simulation (HAES) program that multidisciplinary, multisensor types of measurements are required on atmospheric disturbance phenomena in order to obtain the requisite data input for application to the description of equivalent types of high altitude nuclear burst induced disturbances, considerable effort was made before, during, and after the field exercise to ensure cooperation between different experimental groups. Hence, we believe that the data obtained and described herein will provide valuable correlative input to a number of experiments, including those related to ICE CAP infrared emission, radar clutter and scintillation experiments and the D-region partial reflection measurements made by ITS.

II. EXPERIMENTAL RESULTS

A. Operational Summary

The Chatanika field site was manned on three separate occasions: 7 to 13 February 1973 to inspect the site, locate and install the optics van; 26 February to 8 March, to conduct preliminary operations and calibrations of the apparatus; and 19 March to 3 April 1973, to conduct the ICE CAP supporting experiments as well as to obtain correlative background data with the Chatanika incoherent scatter radar.

Photometric data obtained during these experimental operations is summarized in Table I. Appendix 1 contains synopses of the operational procedures and auroral conditions on a day-by-day basis during this period.

Two photometers were operated simultaneously during most of the observing periods:

- o The trichroic photometer, to monitor energy deposition and ionospheric response in the 4278Å, 5577Å, and 6300Å spectral regions;
- o The three beam photometer, which was intended to detect structured auroral features, wavelike and turbulent like irregularities in the D-, E-, and F-regions by monitoring 5890Å, 5577Å and 6300Å emission intensity fluctuations respectively.

The pertinent characteristics of the photometers are summarized in Table II. Unfortunately, full azimuth elevation scan capabilities could not be provided to the trichroic photometer unit, which degraded its capabilities to support some ICE CAP and other experimental operations.

Photometer calibration with the radioactive light source was done on a daily basis as described in reference 1. Calibration factors pertinent to the ICE CAP data are summarized in Table III. Additional calibrations were undertaken using the AFCRL LDF tungsten light source. A detailed comparison of these data with the LMSC calibration source has not been completed as yet.

TABLE I

ICE CAP '73 ALASKA OPERATIONS SUMMARY

	Tape-File	Date	Hours-UT	Photometers	Conditions
	I-1	2-29	0950-1355	3-C	Pulsating forms
	I-2	3-2	0710-0901	3-C	Hazy & cloudy
			1050-1304	3-C & scans	Very active
*	II-1	3-3	0500-1355	3-C & 3-B	Very active
*	II-2	3-4	0535-1209	3-C & 3-B	Quiet
	III-1	3-5	Calibration test tape		
	V-1	3-20	0832-1143	3C & 3B	No activity
	V-2	3-21	0500-1327	3C & 3B	Very active
					OH rocket
	VI-1	3-22	0530-1310	3C & 3B	Active forms
					BB launch
	VI-2	3-23	0545-1416	3C & 3B	Arcs present
	VII-1	3-24	0615-1110	3C & 3B	Variable thin clouds
	VII-2	3-25	0647-1033	3C & 3B	Arcs and breakup
	VIII-1	3-26	0630-1125	3C & 3B	Good red structure
					stopped because of haze
	VIII-2	3-27	0540-1345	3C & 3B	Breakup observed
	IX-1	3-28	0645-1226	3C & 3B	Pulsating aurora
	IX-2	3-29	0717-1316	3C & 3B	Hazy and cloudy, some data
*	X-1	3-30	0600-1318	3C & 3B	Very intense & breakup
*	X-2	3-31	0530-1223	3C & 3B	Arcs and breakup
	XI-1	4-1	0700-1306	3C & 3B	Strong arcs & breakup
	XI-2	4-2	0700-1230	3C & 3B	Fast pulsating auroras

* These tapes have not been converted successfully into useable computer formatted data as yet.

Table II
PHOTOMETER SPECIFICATIONS

Field of View	
Trichroic Photometer	3°
3-beam Photometer	1° centered on 8° equilateral triangle
Wavelengths	
Trichroic	4278Å, 5577Å, 6300Å simultaneous
3-beam	5577Å, 6890Å, 6300Å sequential
Time Resolution	0.4 to 1.0 seconds
Orientation	
Trichroic	Any zenith angle in magnetic meridian
3-beam	Magnetic zenith (Az 204, el 79)
Sensitivity Range (typical)	
Trichroic	1 to 10^5 Rayleighs
3-beam	10 to 10^5 Rayleighs

Table III

ICE CAP CALIBRATION FACTORS FOR ENERGY DEPOSIT

Wavelength (A)	Passband (A)	Sensitivity (R/ct)	Energy Calibration Factor (ergs $cm^{-2} sec^{-1} R^{-1}$)
4278Å	67 Å	6.7 ± 2.3	4.7×10^{-3}
5577Å	6.0Å	11.5	--
6300Å	5.7Å	1.8	--

B. ICE CAP Energy Input Data

Photometric data relating to energy input in the vicinity of the rocket E-region penetration point were obtained for four ICE CAP rocket experiments, as summarized in Table IV. As previously pointed out, the photometer scan orientation is confined to a single meridian plane, and due to misinformation with respect to rocket trajectories received during van installation, it proved impossible to cover the 40° East azimuth rocket trajectory area. ICE CAP operations of the trichroic photometer therefore were limited to the magnetic meridian at a zenith angle of 10°. The data discussed herein will thus be indicative of the auroral conditions in the vicinity of the rocket trajectory but will not provide a precise quantitative picture of precipitating particle energy deposition, immediately about the trajectory. Fortunately, the LMSC Image Intensified TV (IITV) camera system was being operated during several of the four ICE CAP nighttime rocket launches, and will provide the complementary spatial data on electron and proton precipitation. Hence, photometric data will provide useful calibration for the IITV data in addition to providing high time resolution energy deposition data.

Calibrated photometric intensity data for the five minute periods surrounding rocket launch times are illustrated in figures 1 through 4b. The particle energy deposition vs. time computed from the 4278Å intensities are also illustrated.

Both the photometric intensities vs. time in the various spectral regions and the energy input plots illustrate the great time variability of the visible phenomena. An additional important characteristic of the auroral events however, is that the visible features are superimposed upon a more diffuse, but still intense background of particle precipitation and energy deposition. This background feature may provide as much or more total energy to a given region of the ionosphere over a period of a few 10's to 100's of seconds as the visible features. Thus, any infrared emission processes which depend upon storage of energy in chemically active or excited states of ambient species over the same time frame may depend

TABLE IV

Date GMT	Launch Time GMT	Intensity at Launch (Rayleighs) 4278Å	5577Å	Average Energy Flux at Launch (ergs $cm^{-2}sec^{-1}$)	Integrated Energy Flux Prior to Launch (ergs cm^{-2}) 10 Min.	60 Min.
21 March	1011	1.5 k	4 k	7.0	4.5 k	30 k
22 March	1213	3.5 k	10 k	16.4	10 k	40 k
24 March*	1031	4 k	20 k	20	11 k	**
27 March	0938	2 k	7 k	9.6	9.2 k	18 k

* Data taken through thin cirrus and/or haze. Actual values of intensities may be in error.

** Data not available for entire period due to clouds.

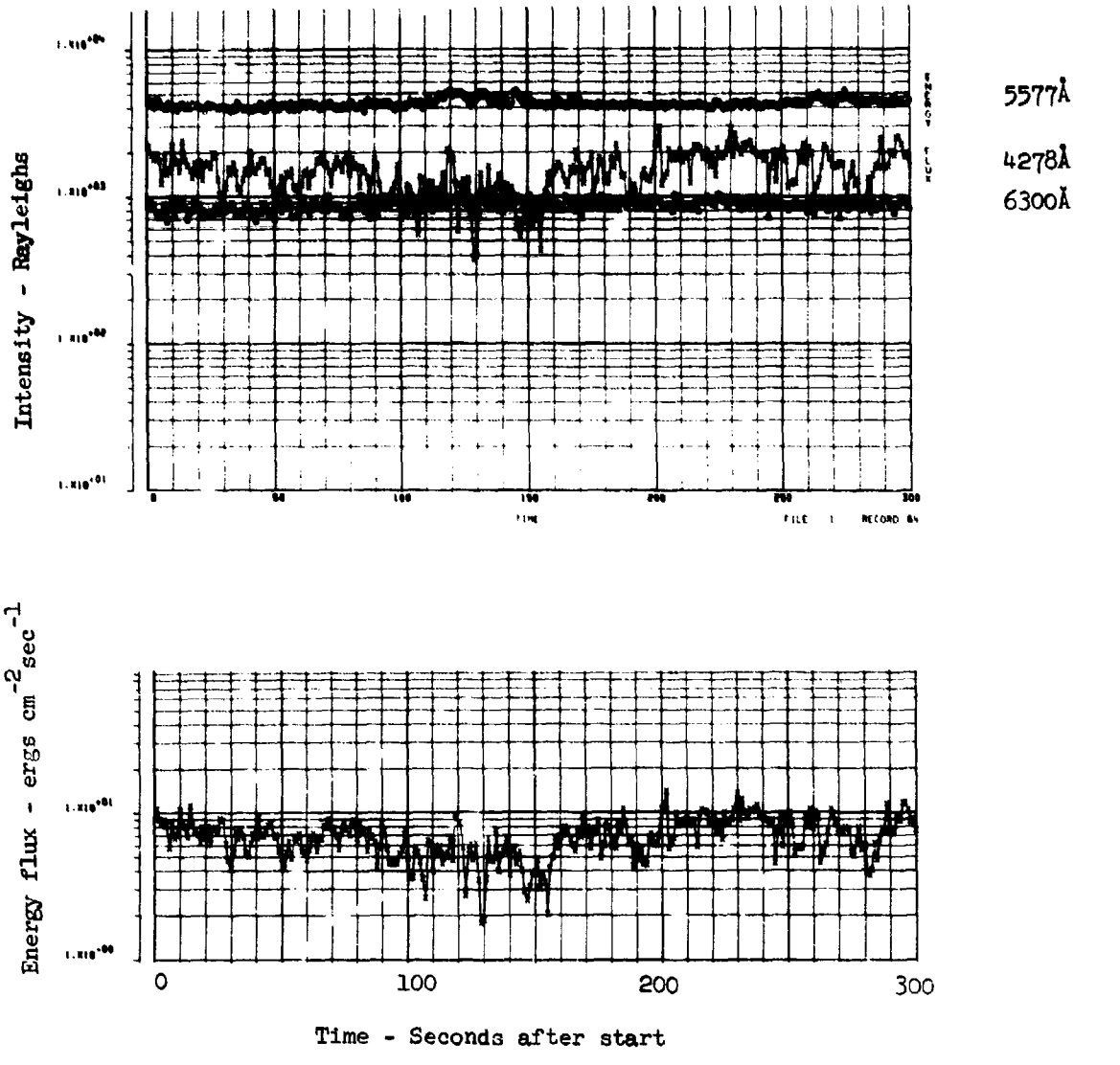

Figure 1 Calibrated photometric intensities and energy flux data for ICE CAP 1973 launch at 1011 UT, 21 March. Beginning time of record is 1010:14 UT.

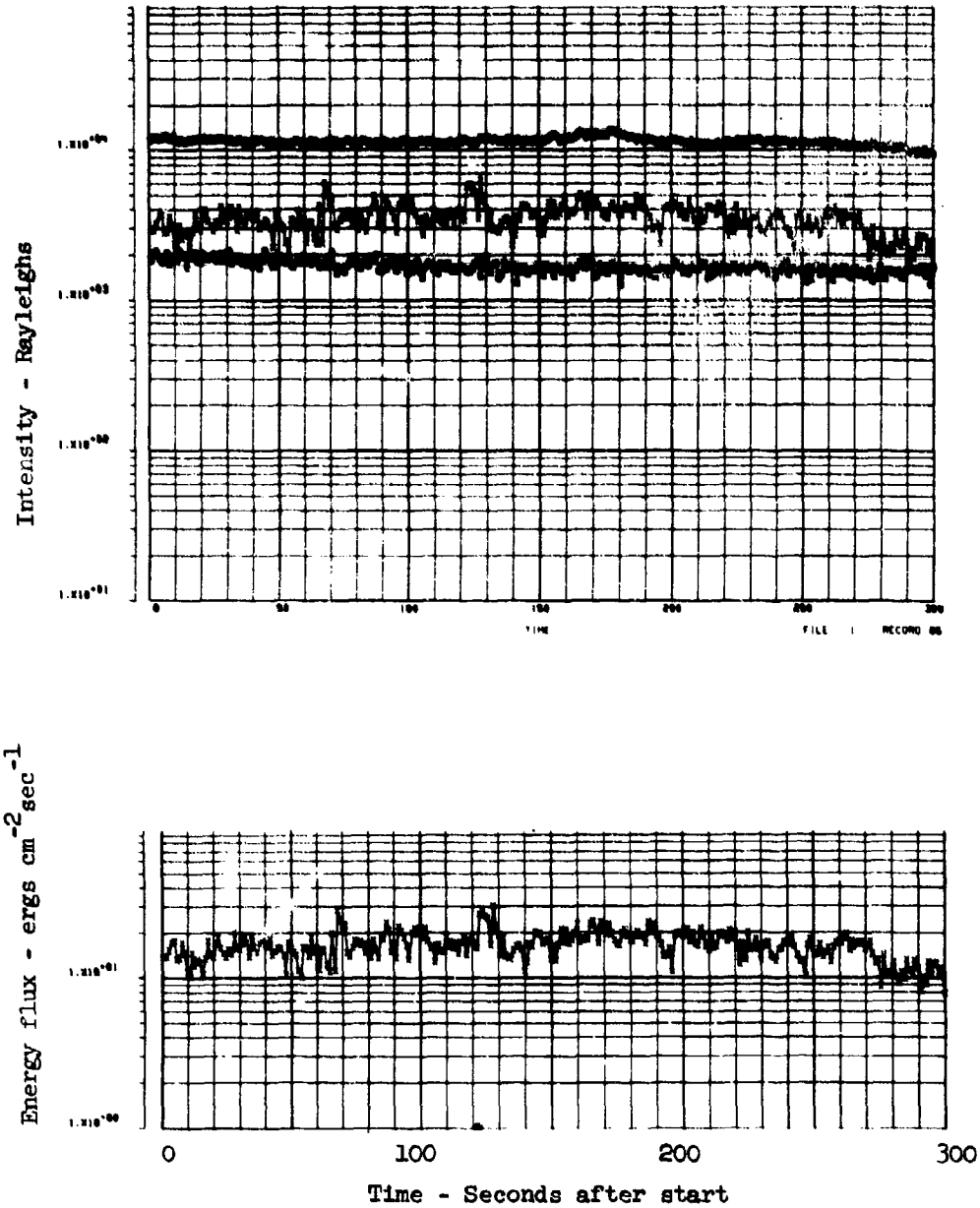

Figure 2 Calibrated photometric intensity and energy flux data for ICE CAP 1973 launch at 1213 UT, 23 March. Beginning time of record is 1213:14 UT.

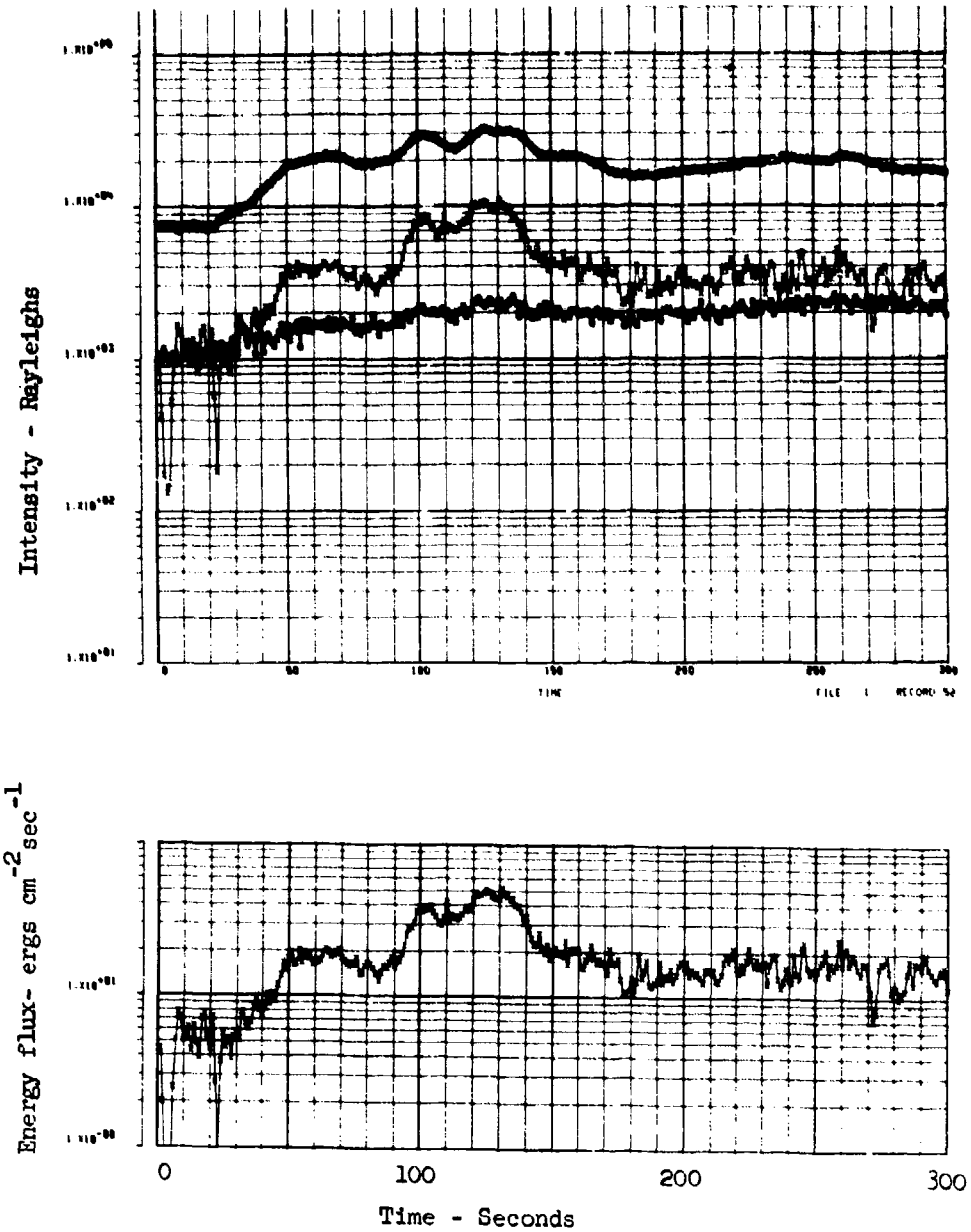

Figure 3 Calibrated photometric intensities and energy flux data for ICE CAP 1973 launch at 1031 UT, 24 March. Note: During this period thin clouds and haze make calibrations' accuracy doubtful. Beginning time of record is 1030:04 UT.

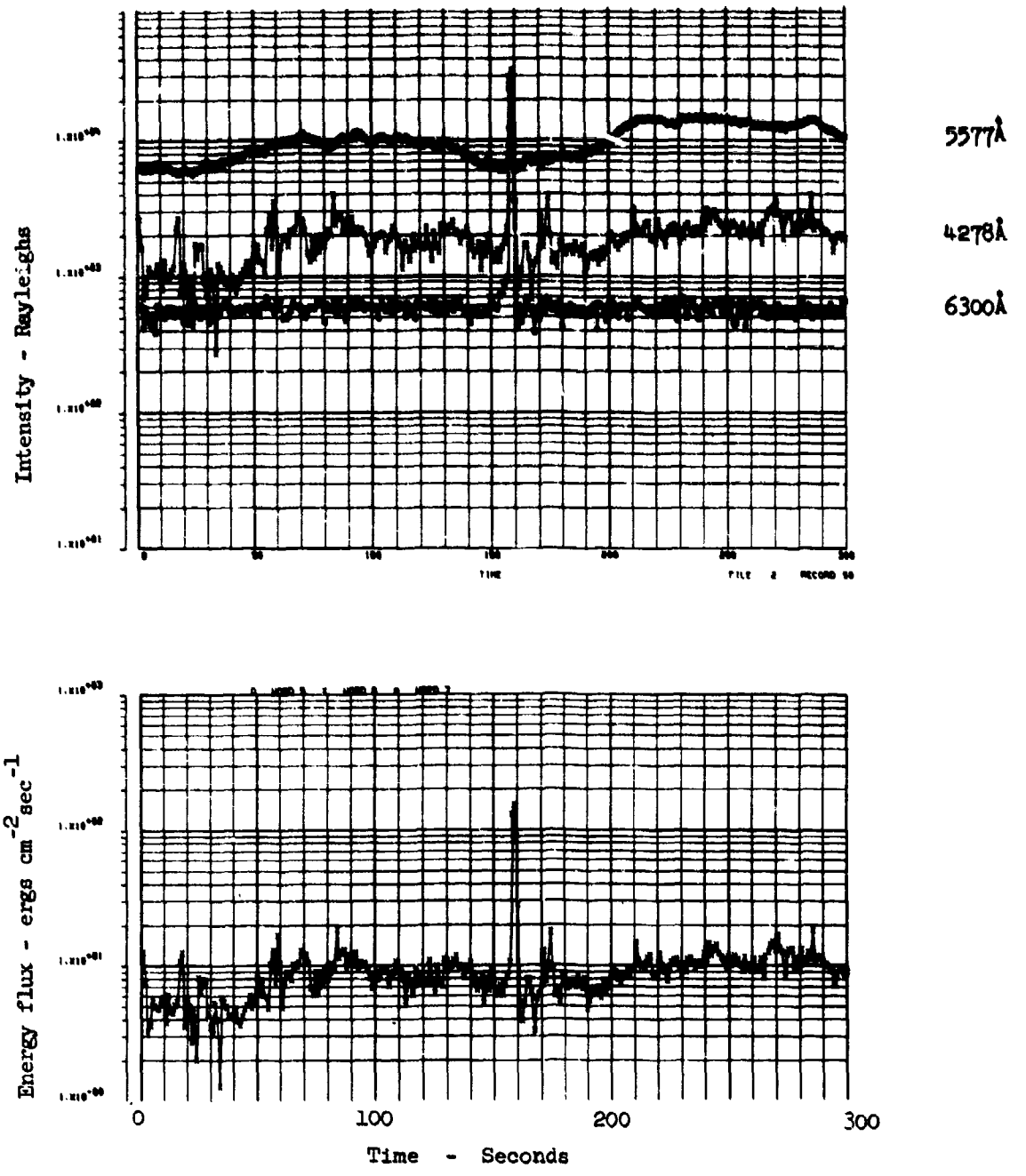

Figure 4a Calibrated photometric intensities and energy flux data for ICE CAP 1973 launches at 0937 and 0938 UT, 27 March. Record start time is 0935:25 UT transient at +159 seconds is PT second stage.

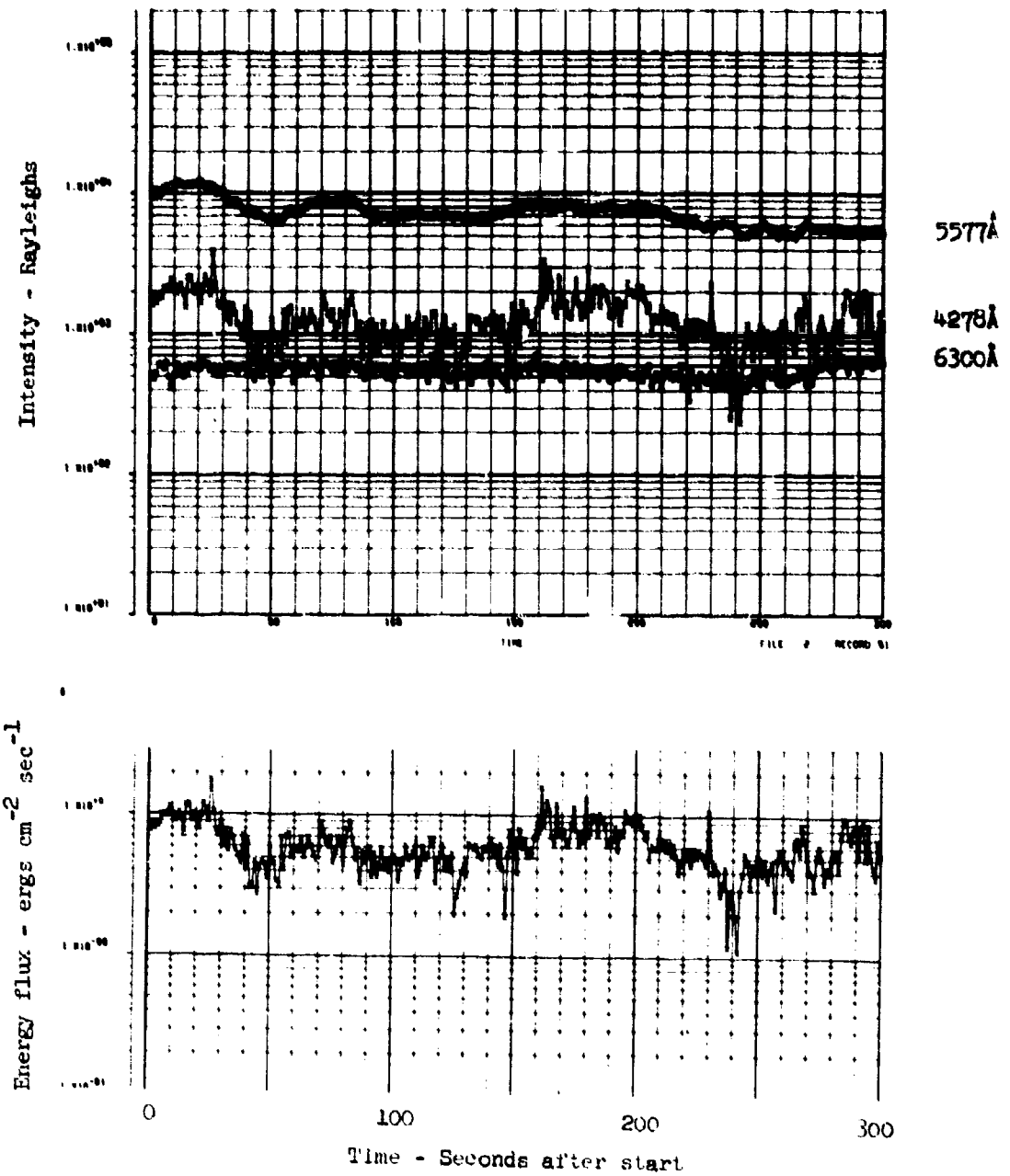

Figure 4b Calibrated photometric intensities and energy flux data for ICE CAP 1973 launches at 0937 and 0938 UT. Beginning time of record is 0940:13, following both launches.

as much or more upon the diffuse background features as upon the visible emission features.

Because the energy storage time is certainly different for different excitation mechanisms and for different IR active species, a useful data presentation is the integrated energy deposited in the field of view of the detector vs. time measured backwards from the rocket observing time. Figure 5 illustrates these data for the ICE CAP events. Clearly, for some, if not all event times, an energy integration time of only a few minutes would suffice to smooth out the relatively large temporal fluctuations in intensity represented by the active visible auroral forms.

Information on the spatial distribution of particle precipitation during the rocket experiments may be obtained from the normal all-sky camera photographs, but in much greater detail from the LMSC IITV all-sky camera, which was operated at Chatanika by Drs. S.B. Mende and R.H. Eather. This apparatus, which will be described elsewhere obtains time resolved photographs of the auroral sky in 4278Å, 4861Å, 5577Å and 6300Å wavelength on approximately a second by second basis (depending upon auroral intensity). TV frames (provided by S.B. Mende) appropriate to the March 24, 1973 rocket experiments are illustrated in figure 6. Utilization of these data plus the photometric data for calibration and increased time resolution, will allow a complete picture of the particle precipitation energy and type to be formulated.

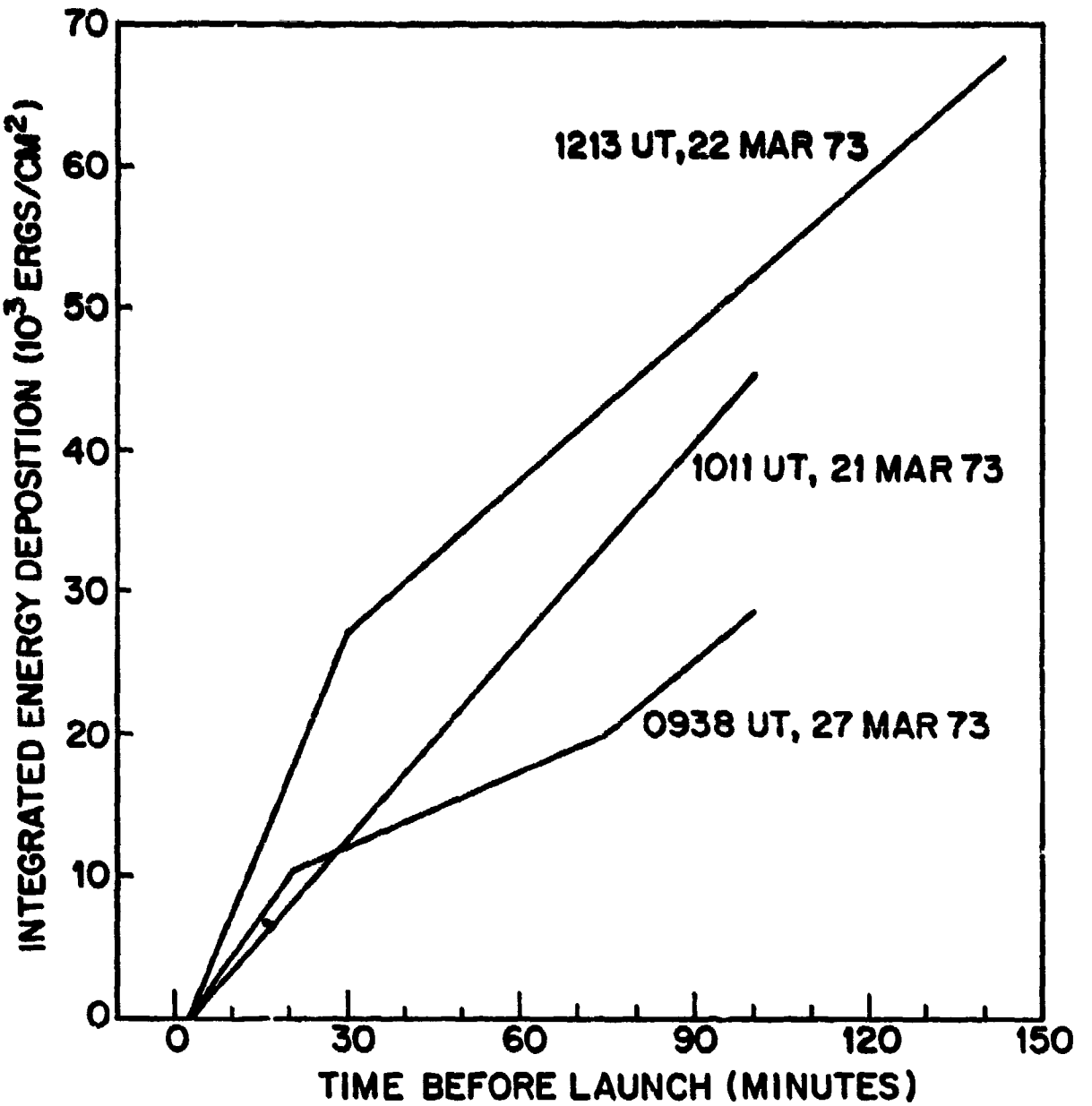

Figure 5 Integrated energy fluxes from precipitating particles vs. time before launch. ICE CAR experiments 21, 22 and 27 March, 1973

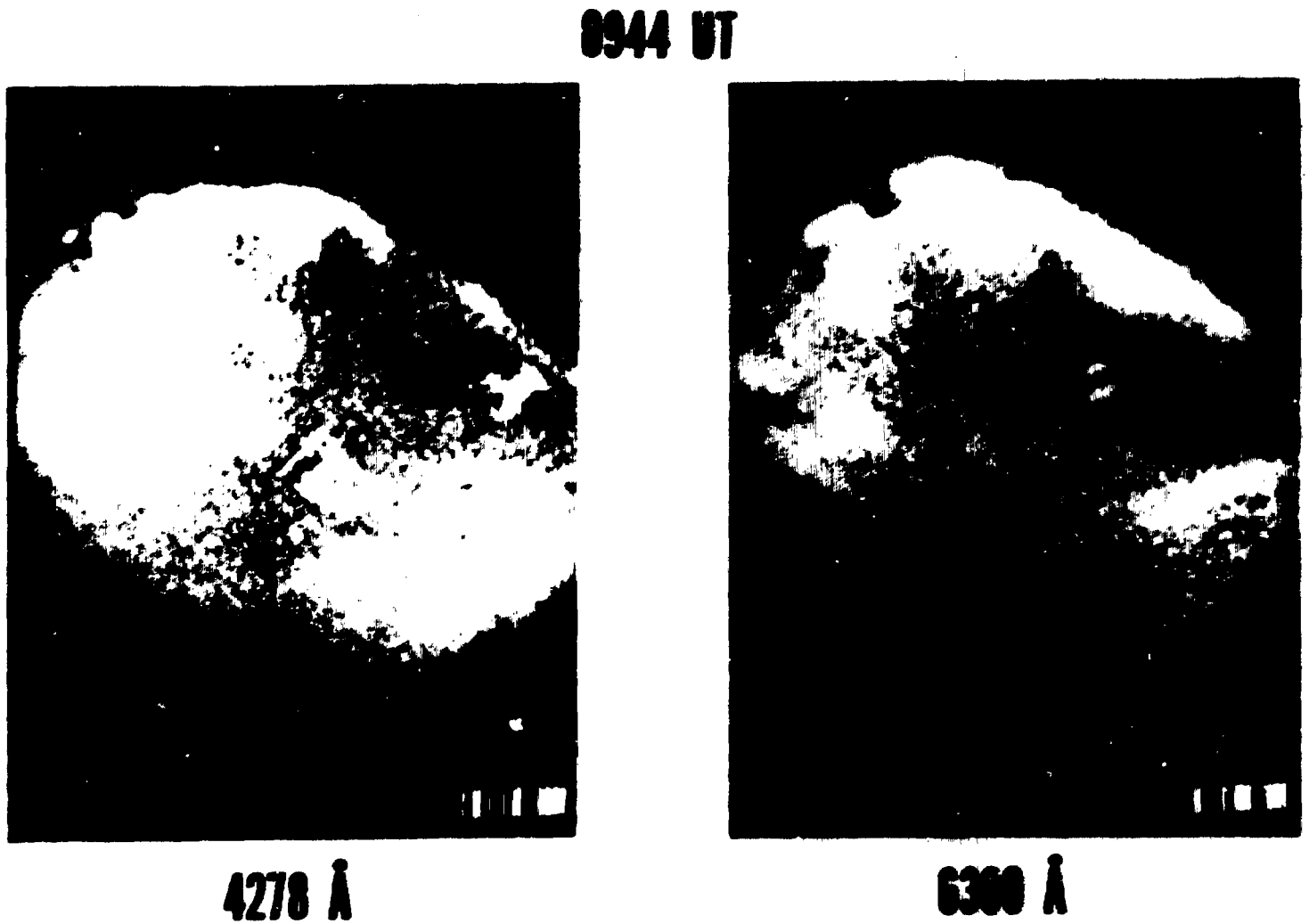

Figure 6 IITV all-sky map (150°) of precipitating energetic particle flux (4278Å) and soft energy particle flux (6300Å) for ICE CAP experiment on 24 March 1973. (Provided by S.B. Mende)

III. ANALYTICAL RESULTS

A. Coordinated Radar-Photometer Experiment on $O(^1S)$ Excitation and Deionization Chemistry

During portions of the 1973 experimental operations at Chatanika, the incoherent scatter radar and the photometers were operated with boresighted fields of view oriented at magnetic zenith. Radar measurements of electron density vs. height and time were made with time resolutions varying from about 2 to 10 seconds. Photometer measurements of auroral emission intensities in the 4278Å, 5577Å, and 6300Å spectral regions were made with time resolutions of 0.4 and 1 seconds. The fast mode was used to record fast fluctuations in active and pulsating auroras. A wide variety of auroral conditions was encountered during these intervals of coordinated measurements ranging from subvisual, quiet arcs to IBC class III active type B and pulsating auroras.

A number of goals were set for the coordinated measurements:

- o To determine the effective electron-ion recombination coefficient under a variety of auroral conditions and intensities,
- o to determine the degree to which the auroral green line at 5577Å is excited by dissociative recombination of O_2^+ and/or by other fast processes,
- o to determine the importance of transport of energy and excited species in auroras under a variety of conditions.

The theoretical and analytical bases for the first experiment were described by Baron (4). This theoretical approach relating the intensity fluctuation spectrum of 4278Å emissions and the electron density fluctuation spectrum was extended to include excitation processes resulting in 5577Å emission. Transport of ionization and excited species may be inferred from both radar drift measurements, and from photometric data.

The equations relating electron density at a given altitude to the source, loss, and radiative excitation and emission of 4278Å and 5577Å wavelengths are as follows:

1) $$\frac{dN_e}{dt} = Q_o - \alpha_o N_e^2$$

2) $$\frac{d\, I_{5577}}{dt} = A_{32}\left[Q_1 + \alpha_1 f N_e^2 - \frac{I_s}{A_{32}\,\tau_1}\right]$$

3) $$I_{4278} = k_o Q_o = k_1 Q_1,$$

where

I_i denotes the intensity at wavelength i (Rayleighs).

ζ_i^2 is the power spectral density of the intensity fluctuations (Rayleigh^2/Hz).

N is electron density (cm^{-3}).

η^2 is the PSD of electron density fluctuations ($el^2 cm^{-6} Hz^{-1}$)

[O(1S)] is the density of the oxygen 1s state.

$A_{32} = 1.4\ sec^{-1}$ is the Einstein radiative transition probability for the O(1s) state.

Q_o is the ionization source term (ion pairs $cm^{-3} sec^{-1}$).

Q_1 is the rate of direct excitation of the O(1s) state ($cm^{-3} sec^{-1}$).

$f = [O_2^+]/N_e$ is the fractional ionization content of O_2^+.

$\alpha_o = 2 \times 10^{-7}$ is the average effective electron-ion recombination coefficient ($cm^3 sec^{-1}$)

$\alpha_1 = 2 \times 10^{-8}$ is the recombination coefficient for the process $O_2^+ + e \rightarrow O + O(1S)$ ($cm^3 sec^{-1}$).

$\tau_1 = (A_{32} + Q)^{-1}$ is the effective lifetime of O(1s) state.

Q is the quenching rate of the O(1s) state (sec^{-1}).

$\tau_o = (2\alpha_o N_e)^{-1}$ is the effective lifetime of total ionization (sec).

$\tau_2 = (2\alpha_1 f N_e)^{-1}$ is the effective lifetime of the O_2^+ dissociative recombination process which results in excitation of O(1s) states (sec).

k_o is the ratio of 4278Å emission to the source strength Q_o (Rayleighs/ion pair sec^{-1}).

k_1 is the ratio of direct excitation of O(1s) to 4278Å emission.
w is angular frequency (radians sec^{-1}).

The relationship of the power spectral densities (PSD) of the time fluctuations in electron density to the PSD of 4278Å emission intensity developed in reference 4 is

$$4) \qquad \eta^2 = \frac{\tau_o^2}{k_o^2} \quad \frac{1}{(1 + w^2 \tau_o^2)} \quad \zeta^2_{4278}.$$

Using a similar method on equation (2), the PSD's of 4278Å, 5577Å, and electron density fluctuations are related by the expression

$$5) \qquad \zeta^2_{5577} = [k_1^2 \zeta^2_{4278} + \frac{\eta^2}{\tau_2^2}] [\frac{A_{32}^2 \tau_1^2}{(1+w^2\tau_1^2)}].$$

Substituting equation (4) into equation (5), the electron density PSD is removed resulting in the following:

$$6) \qquad \zeta^2_{5577} = \zeta^2_{4278} [k_1^2 + \frac{k_o^2 \tau_o^2}{\tau_2^2} (\frac{1}{1+w^2\tau_o^2})][\frac{A_{32}^2 \tau_1^2}{(1+w^2\tau_1^2)}].$$

The above equations apply strictly to the case wherein electron density and emission intensities are related to volume changes. However, for the case where ionization and emission from a constant thickness layer is considered, the above equations also apply and the time constants and other parameters of the model are to be considered as averages over the layer.

Further simplification of equation (6) results from adopting the known relationships between some of the parameters, particularly the time constants τ_o and τ_2. Because the total effective recombination

coefficient α_o is a known multiple of the coefficient for O_2^+ recombination (with associated O(1s) excitation), i.e. $\alpha_o = 10\,\alpha_1$, then the ratio $\tau_o/\tau_2 \sim f/10$ and equation (6) becomes

$$7) \qquad \zeta^2_{5577} = \zeta^2_{4278}\left[k_1^2 + k_o^2\,\frac{f^2}{100}\,\frac{1}{(1+w^2\tau_o^2)}\right]\left[\frac{A_{32}^2\,\tau_1^2}{1+w^2\,\tau_1^2}\right].$$

Equation (7) can be further simplified according to the frequency range of the data. For low frequencies, $w \ll \tau_o^{-1} \ll \tau_1^{-1}$ the ratio of 5577 to 4278Å PSD's becomes constant as shown in equation (8).

$$8) \qquad R = \zeta^2_{5577}/\zeta^2_{4278} = (k_1^2 + \frac{k_o^2 f^2}{100})\,(A_{32}^2\,\tau_1^2).$$

In this equation, $k_o = 60$ is a known quantity, the factor $(A_{32}\,\tau_1)$ is unity if there is no excess quenching of the O(1s) state, and decreases to values about 0.5 or so for typical auroras. The value of f, the ionization fractional content of O_2^+ is always less than or equal to unity. Using these physical relationships it can be shown that the value of the parameter k_1 must be always less than or equal to the value of $R^{1/2}$. It appears that under most physical circumstances, the value of the second term in expression (8) will always be negligible compared to the k_1^2 term, hence, the low frequency ratio of 5577Å to 4278Å PSD's will be a measure of the ratio of direct excitation of 5577Å emission by fast processes to 4278Å excitation, weighted by the quenching factor for the O(1s) state.

Several test cases have been computed to evaluate the power spectral density technique for determination of the ionospheric O(1s) state excitation, quenching, and deionization coefficients. For a variety of reasons, these test cases do not include the times of ICE CAP rocket experiments which will be processed during the ICE CAP analysis program. Two auroral types were processed: a very intense and active aurora IBC class III, type B, and a pulsating aurora (period about 5 seconds) of

average intensity about 10kR in 5577Å (IBC class II). In the later case, use of the SRI/LMSC derived theory, presented herein, is quantitatively justified to the approximation limits of the perturbation technique. For the large scale active aurora, the ionization changes were large compared with the average ionization density; hence, the perturbation technique is probably not justified in detail. This aurora was studied however to see if any effect of the second term of equation (6) could be detected insofar as this term is the one dependent upon linearization of the ionization continuity equation (eqn. 1).

Figure 7a and 7b illustrate the intensity vs. time plots for the two auroral cases, for the 4278Å and 5577Å spectral regions. These data were treated as time series, the correlation functions, coherence, power spectral densities, and relative phase angles were computed as described in Appendix 2. Figures 8 through 10 illustrate pertinent results from these computations.

The calibrated power spectral densities are presented for both auroral cases in Figure 10. Here, it is clear that at the lower frequencies, the PSD ratios are nearly constant, in qualitative agreement with the predicted behavior in equation (8). In the case of the pulsating aurora, the value of k_1, the ratio of direct O(1s) state excitation to 4278Å emission is equal to or greater than 1.7 times the quenching factor. In the case of the active aurora, the PSD radio is not as constant, but the PSD ratios tend to be smaller indicating a value of k_1 about 1.2 times the O(1s) quenching term value.

The PSD plots can be interpreted in terms of the quenching lifetime also. If we take the frequency at which the difference between 5577Å and 4278Å PSD's becomes negligible, then we see that the equivalent lifetime values are about 1.8 and 1 seconds for the active intense and the pulsating auroras respectively. Both of these values are approximate, but both exceed the expected radiative lifetime of the O(1s) state which is 0.7 seconds. This behavior was predicted by Brekke (5) and for cases in which

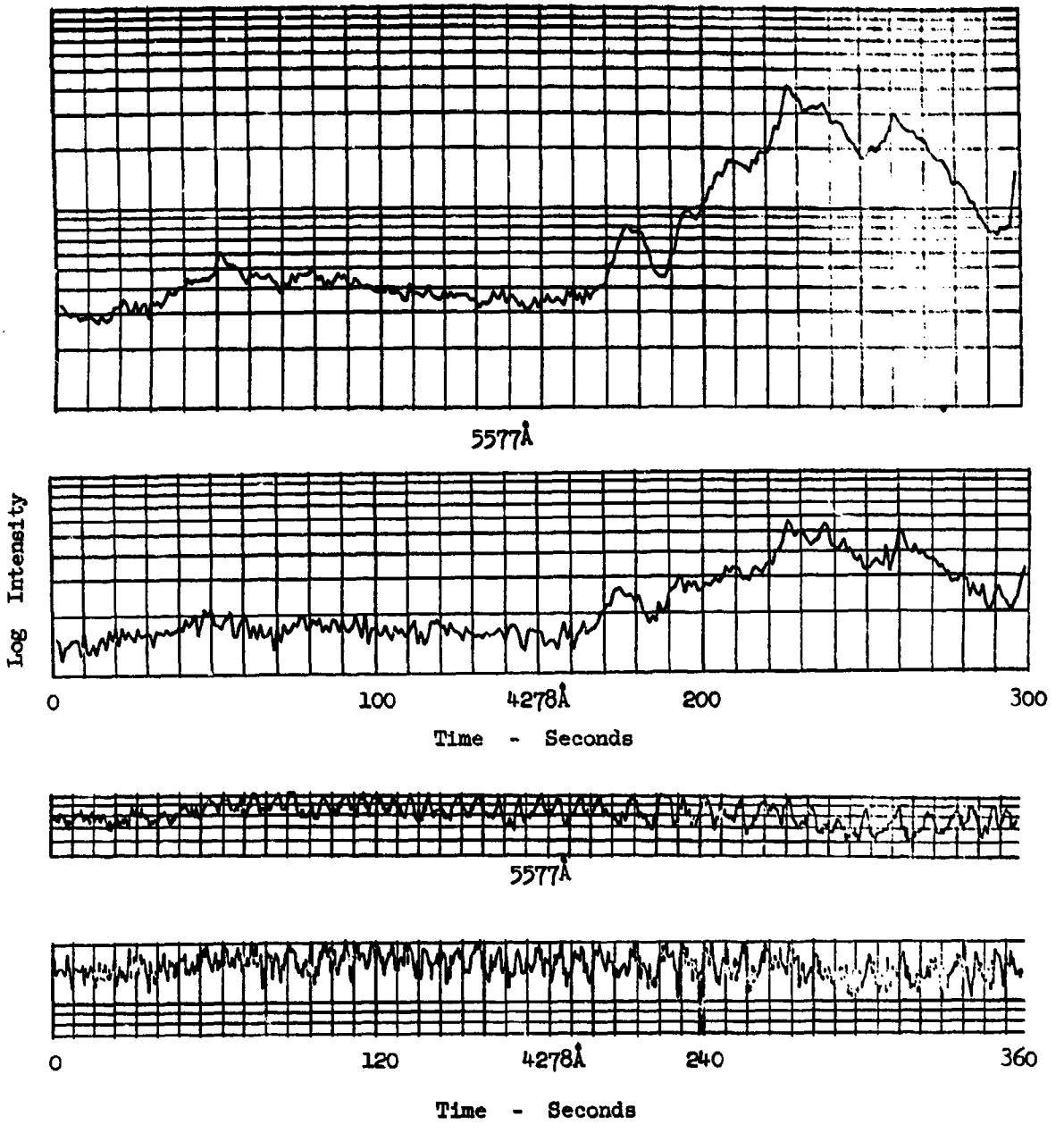

Figure 7 Relative intensity vs. time plots for 5577Å and 4278Å emissions in intense IBC III aurora (above) and IBC II pulsating aurora (below). Rate pulsation period 5-10 seconds.

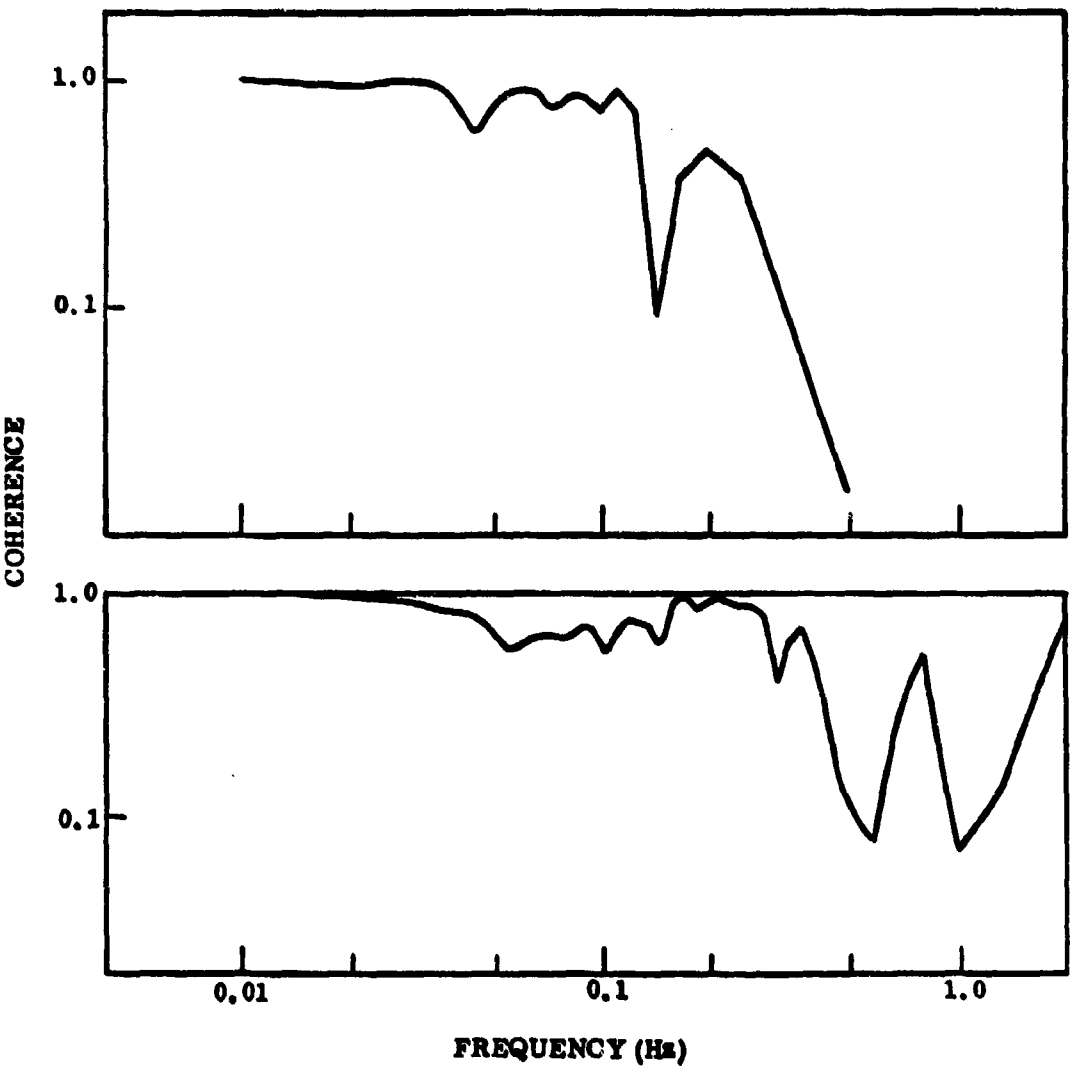

Figure 8 5577Å and 4278Å intensity fluctuation. Coherence vs. frequency for two auroral cases. Top curve illustrates IBC III aurora. Bottom curve is for pulsating aurora.

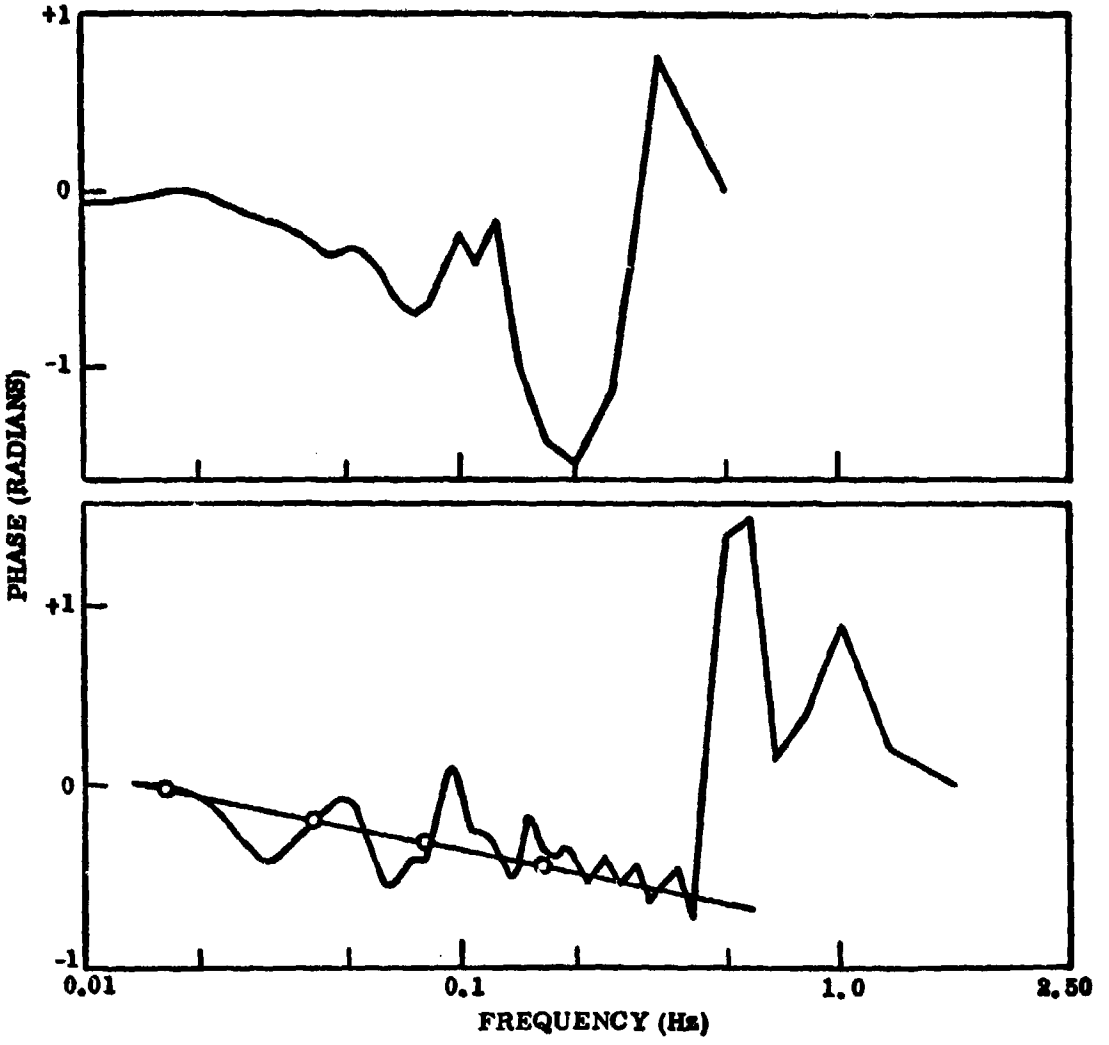

Figure 9 Phase angle vs. frequency for fluctuations at 5577Å and 4278Å intensity for intense auroral form (upper) and for pulsating aurora. The O(^{1}S) lifetime and excitation - de-excitation processes' rates may be inferred from these data.

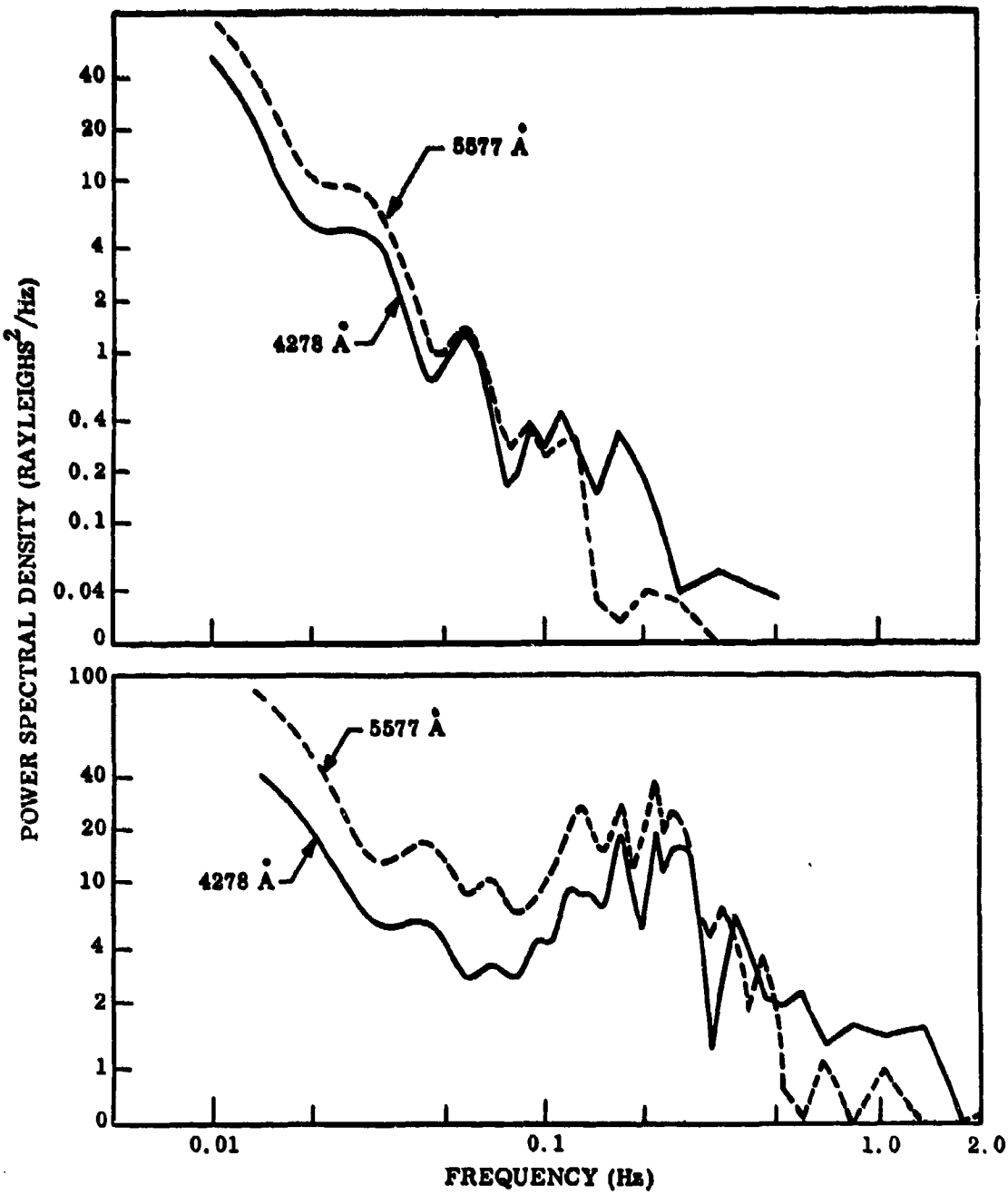

Figure 10 PSD's of emission intensity fluctuations for two types of auroras; type B class III (above) and class II pulsating (below).

secondary excitation processes were present in addition to the direct excitation processes which correlate completely with 4278Å emission.

These time constants may be verified by adopting the method of Omholt (Ref 6) and plotting the tangent of the phase angle vs. angular frequency. The time constant is then given by the slope of the plot. Two cases, corresponding to the intense active aurora and the pulsating aurora are illustrated in figure 9. The time constants computed are 1.0 sec and 1.4 sec respectively, which correspond closely to those deduced from the PSD plots. These test cases indicate that the statistical computations can provide useful data on the physical processes which excite the 5577Å emission as well as on the quenching time of the O(1s) state. However, more computations must be carried out, and more cases studied, before applying this technique to evaluation of ICE CAP '72 and '73 ionospheric processes.

B. Analytical Prediction of Expected Radar Degradation at Kwajalein Missile Range from Observed F-Region Optical Structure

As an example of the potential application of ionospheric optical emission irregularity data to prediction of radar propagation effects, we have computed some expected radar degradation effects based upon low latitude optical data on F-region structure. At low latitudes, the F-region strongly emits the 6300Å OI line which has been shown to result from the reaction $O_2^+ + e \rightarrow O^* + O^*$. Hence, the emission intensity, and its spatial structure are strongly correlated with the F-region electron density and its spatial structure. This relationship has been utilized to predict the changes in integrated electron density along a radar propagation path which result from 1) gross F-region structure, and 2) fine scaled structured features (e.g. spread F).

KMR lies just to the north of the geomagnetic equator, near the edge of the daytime equatorial electrojet. The region viewed by KMR tracking radars extends eastwards towards Hawaii, and intersects much of the region which Appleton called the equatorial ionospheric anomaly. Figure 11 illustrates the pertinent geometry.

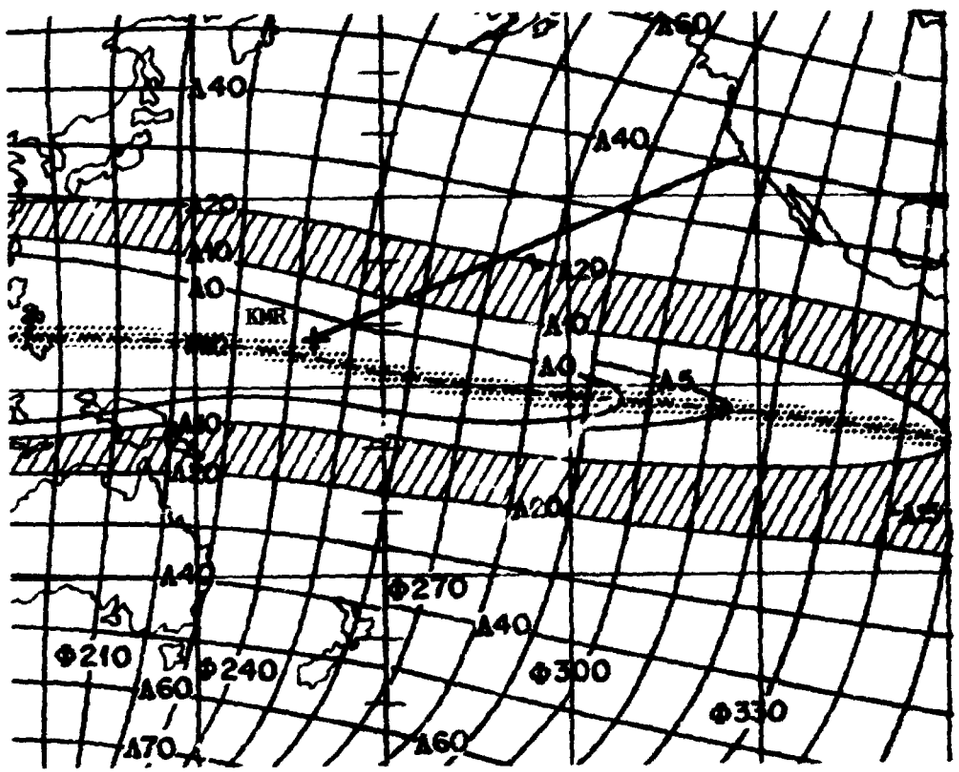

Figure 11 Location of KMR and PMR missile trajectories with respect to electrojet and intertropical arc locations.

The equatorial ionospheric anomaly discovered by Appleton is characterized by bands of enhanced ionization density in the F-region at approximately 15 degrees north and south of the geomagnetic equator. These bands have localized structure and their synoptic morphology is much different than the temperate latitude ionosphere, hence their designation as anomalous. Barbier (7) discovered that bands of enhanced emission of the OI, 6300Å line overlay the latitude location of the ionization bands. Barbier, Roach, and Steiger (8) discovered the physical connection between these phenomena, namely that the red emission is excited during dissociative recombination of the ionization in the enhanced or anomalous region. This physical relationship allows a direct map of ionospheric F-region structure to be derived from photometrically observed structured red emission features.

Imbedded in the average enhanced ionization-emission arcs are smaller scale irregularities. These range from corrugations which are hundreds of kilometers across and which sometimes produce tilts in constant ionization density surfaces exceeding 45 degrees, to small scale striations of a few 100's of meters extent perpendicular, and hundreds of kilometers extent along the geomagnetic field lines. The detailed physical mechanisms underlying these irregularities have not been fully investigated as yet; however, they are known to produce radar backscatter from altitudes as high as 1000 km above the equator, to produce transequatorial propagation ducts for frequencies as high as a few hundred MHz, and to produce a variety of satellite scintillation and ionosonde spread F propagation conditions.

Maps of the ionospheric corrugations have been produced by Roach, Steiger, and coworkers, one of which is illustrated in Figure 12. The emission structure is related in detail to the peak electron density (foF2 parameter) of the ionosphere and to the average height of the F region (h'f) by the formula:

$$9) \qquad Q = K_1 + K_2 \, (foF2)^2 \exp\left(-(h'F-200)/H\right).$$

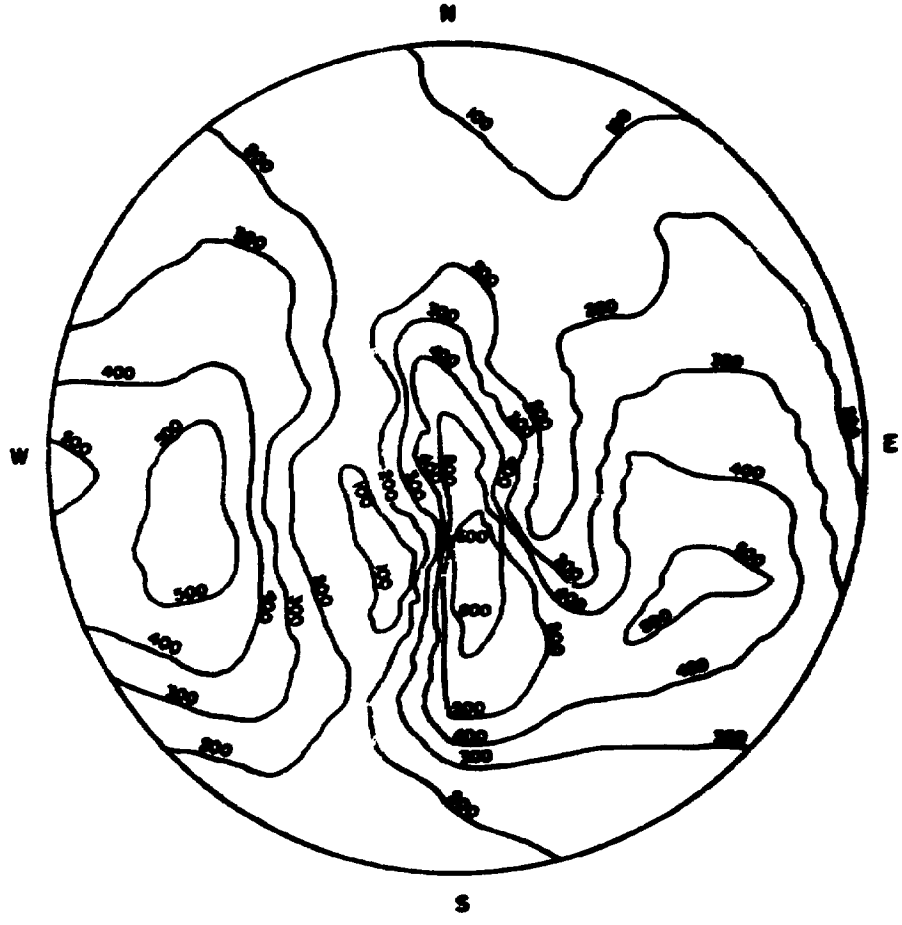

Figure 12 All sky isophote contours of 6300 A, OI airglow from Haleakala showing Toaes and other structured features.

From this formula, the ionospheric density structure and height can be deduced from a photometric map as illustrated in Figure 13. This will be done, and related to radar effects in the next section.

The observed properties of small scale structure imbedded in the corrugations and in the arcs themselves are described in Table V. These properties have some statistical distribution which has not been determined as yet. Likewise, their occurrence pattern is not well known except on a statistical basis. They nearly always are observed at nighttime, seldom at dusk, and during about 50% of the dawns. The physical causes of neither the large scale corrugations nor the small scale striations are known at present.

In order to describe the effects of both large scale corrugations and small scale striations upon radar systems of interest in a general way, we have computed typical values of time rates of change of integrated electron content along some typical radar propagation paths. These parameters then may be used to compute radar range and angle scintillation effects by the reader without detailed description of the radars being required herein.

Two cases are modelled: the photometric structure map illustrated in Figure 12 is converted to an ionospheric structure map through the Barbier formula (in previous section), which is then used to compute approximate values of d INE/dt(electrons/cm^2 column/sec) for a typical tracking case wherein the propagation path passes through the structured region from 5 to 10 degrees elevation angle. We assume the structured region begins 1000 km uprange from the radar, and is 2000 km in extent. Figure 13 illustrates this region, wherein the F layer is modeled by a slab, 80 km thick. We have assumed for this model that the average electron density in the slab remains constant, and that only the average height changes. This case probably is conservative from the radar effect standpoint because no changes in average density are assumed. These would only increase the rate of change of column electron density as the tracking beam moved obliquely through the structured region. The bottom

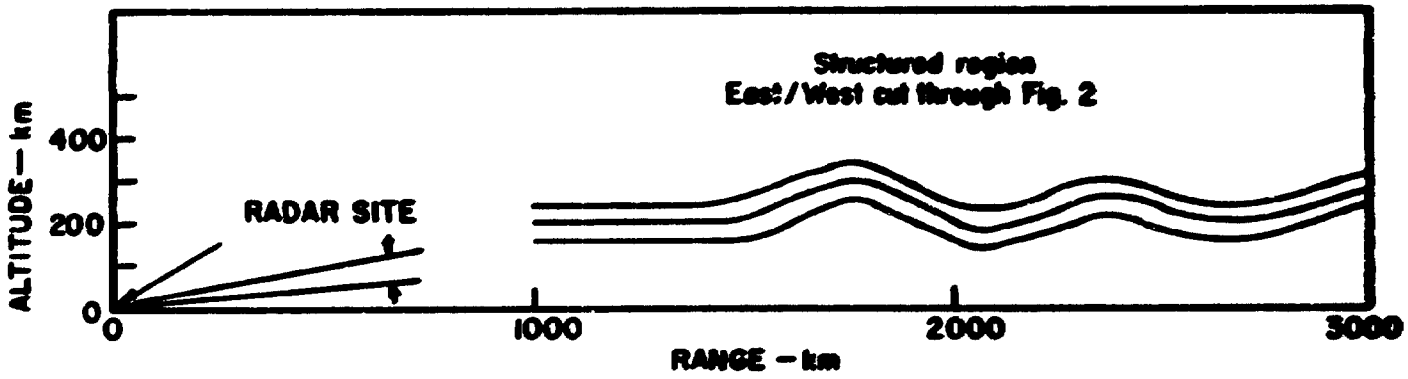

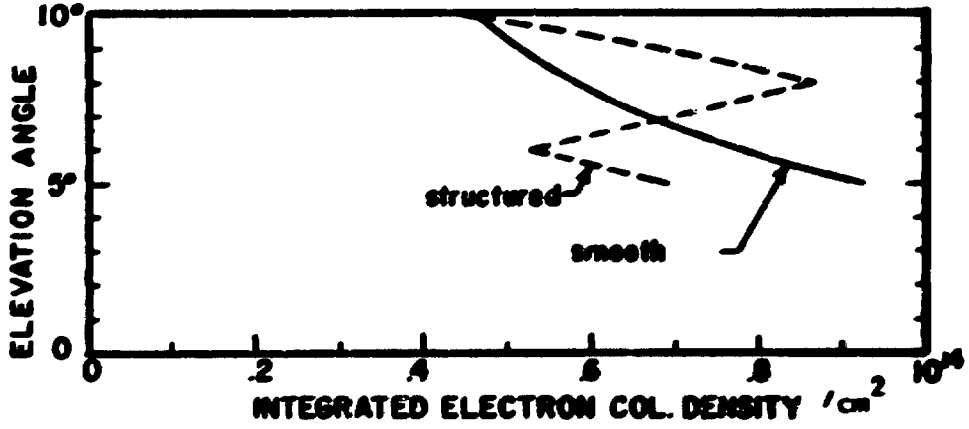

Figure 13 Side view of Figure 2 irregularity placed up range from IDR showing changes of integrated electron content vs. radar elevation angle. The effect of a smooth ionospheric profile is also shown.

Table V

Geometrical Characteristics of F-Region Irregularities

Parameter	Equatorial
Small Scale	
width $\perp B$	10 to 100's m
length $\|\|B$	$\geq$ 1 km
axial ratio	7.5:1 to 100:1
altitude extent	to ~ 1000 km
drift velocities	$\leq$ 100 m/sec E, W
$\Delta N_e/N_e$, form	negative (holes) or positive (sheets) $\approx$ few percent amplitude
Irregularity Patches	
latitude extent	$\leq$ 1000 km
longitude extent	150 to 1000 km
drift velocity	10's m/sec
patch lifetime	10's to 100's of minutes

of Figure 13 illustrates the rate of change of INE (integrated number density of electrons) as an object with velocity 4 km sec^{-1} is tracked through the structured region. A smooth ionosphere comparison curve is also provided. This value of electron density change per second is comparable to that which would be produced by a 10 km thick artificial striation of peak density 10^8 electrons/cm^3, being swept over in 1 second. Because of the different range, tracking rates, and possibly different Fresnel zone sizes, a more direct comparison of the relative degradatory effects cannot be made at this time.

A primitive model of the effects of small scale structure or natural striations is based upon statistical addition of their individual RMS effects. We assume a 5% modulation of a low nighttime electron density of 10^5. The irregularities are of characteristic 1 km size perpendicular to the magnetic field, and a track velocity of 4 km/sec is assumed. Thus, a single irregularity produces an average peak-to-peak change in electron column density of 2×10^9 el/cm^2 sec. If we further assume that the irregularity region is on the average, 40 layers (i.e. 40 km) thick, with the distribution of irregularity centers randomized then adding RMS values of electron column density change produces an effective change of about 10^{10} electrons/cm^2sec. Obviously, for higher average electron densities, such as occur in the peaks of the intertropical arcs and in the corrugations, much higher values of RMS column density fluctuation could occur. Even the natural ionospheric drift motions will produce values of about 10^7 to 10^8 in column density change. For oblique geometry, the effective layer thickness is increased.

C. OBSERVATIONS OF SUBSTORM TIME VARIATIONS IN 4278Å, 4861Å, and 5875Å EMISSIONS DURING THE ICE CAP 1972 EXPERIMENT

A number of investigators have attempted to detect precipitating alpha particles in the auroral regions by means of Helium optical emissions at 5876Å. These investigations have been summarized by Omholt (ref.6). Published observations to date indicate that the incidence of Helium precipitation, at least as evidenced by its optical output, is indeed sporadic and weak. Only Stoffregen (9) has published a spectrum in which the 5875Å He line is identified. However, interpretation of this and other observations are subject to question because of two factors: the magnetic zenith-horizon shift in the doppler line profile has never been observed; and several sources of contamination to the He line are known to be produced by auroras, namely, the (2-2) 1st negative band of O_2^+ and the (9-5) 1st positive band of N_2. Reasoner (10) presents convincing arguments that reproduceable detection of precipitating Helium optical emissions has yet to be achieved.

Auroral region precipitation patterns tend to be organized according to local geomagnetic time and latitude for relatively quiet, non-substorm conditions (see for example, Eather and Mende, 11), and according to substorm time for disturbed periods (Eather and Mende, 12). Concurrent precipitation of protons and alpha particles in discrete events associated with substorms should then provide identifiable phenomenological clues as suggested by Stoffregens observations. In this paper, we show that enhanced 5875Å emission associated with substorm increases in 4861Å Ht emission may be attributed entirely to electron and proton excited contamination emission; namely by portions of the N_2(9-5)1P and O_2^+(2-2)1N bands.

OBSERVATIONS

Auroral intensities in the 4278, 4861 and the 5875Å spectral regions were recorded during the period 7 to 15 March 1972 at Poker Flat, Alaska, between local times of approximately 2000 and 0200. The range of auroral

activity was generally low, between subvisual and IBC II, and the geomagnetic activity did not exceed $K_p = 3+$. During much of the period of observation, only weak auroral forms were observed, superposed upon a diffuse precipitation background which may correspond to the nighttime auroral "Drizzle" region or to Eather's (11) widespread soft zone which predominates in the absence of discrete visible auroral events.

Intensity measurements were made simultaneously in three spectral regions utilizing a trichroic filter photometer and an individual color wheel photometer described by Sears (ref.13). Digital photon counting and recording techniques were used throughout the experiment and the intensities were recorded on a second by second basis for later computer analysis. The pertinent characteristics of the photometer system are summarized in Table VI. The photometers were mounted on an azimuth-elevation scanning mount such that scans in the magnetic meridian could be conducted. During the overall period of observation about 50 hours of simultaneous 4278, 4861 and 5875Å intensity measurements were obtained, about half of which incorporated meridional scans. We have selected approximately 30 of the highest quality 15 minute data periods for the analysis reported herein.

The photometers were calibrated by measurement of the spectral response of the interference filters, and the counting rate produced by a radioactive phospher light source. In all cases, the photometer dark count as well as an estimated stellar and atmospheric continuum emission background count were subtracted. Although the latter was computed on an a-priori basis, the consistent errors in the data are apparently only a few Rayleighs.

Emission intensities for the three spectral regions, 4278, 4861 and 5875Å recorded on six nights of the experimental period are illustrated in figures 14a - 14c. These data may be divided into two groups, based upon whether or not substorms occurred during the observing period. Substorm occurrence was based upon observation of a magnetic bay on either Poker Flat, or Ft. Yukon magnetograms.

TABLE VI

PHOTOMETER SYSTEM PARAMETERS (1972)

Characteristic	Specification
Objective:	7-inch f.l. F2.5 Aero Ektar
Field of View:	
1) Trichroic Photometer, 4278Å/4861Å	3 degrees
2) Fixed Filter Photometer, 5875Å	1°, boresighted to trichroic photometer
Peak Wavelength ± FWHM Passband	4277 ± 15Å
	4877 ± 2.5Å
	4860 ± 30Å
Time resolution for data acquisition:	1 sec
Digital count rate limit:	Dark current to 10^7 counts/sec
Intensity range	10 R to 10^7 Rayleighs (10 sec integration)
Intensity measurement statistical error ± 1 σ (1 sec basis)	4278 1 σ = 10 to 20 R 4861 1 σ = 20 to 50 R 5875 1 σ = 2 to 5 R

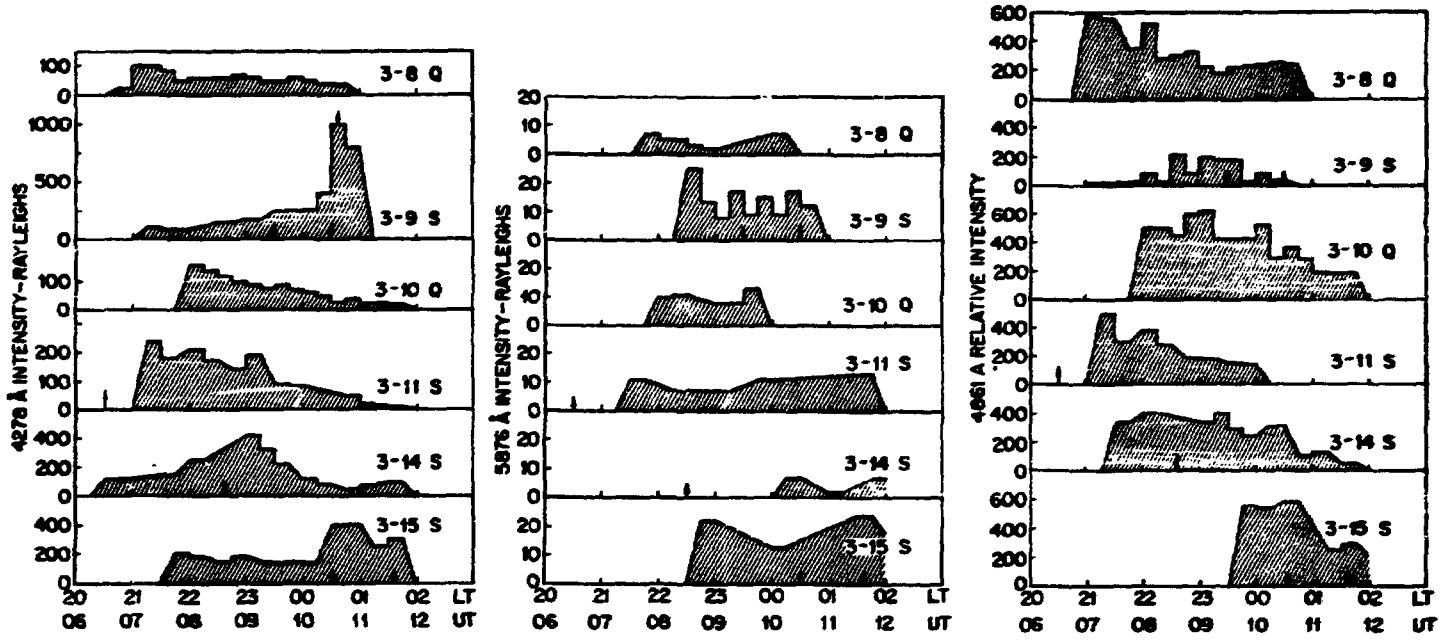

Figure 14 Time dependence of 4278Å, 5875Å and 4861Å auroral emission intensities. Blank areas indicate times at which data were not available, or were considered too poor to use in the analysis. Fifteen minute segments connected by sloped lines indicate times in which data were incomplete, but inferred intensities were consistent with adjacent time segments and with intensities in other wavelengths. Nights which had no magnetic bays during the observing period are indicated as 3-10 Q. Magnetic bays on disturbed dates (eg. 3-15 S) are indicated by arrows.

Emission intensity in the 4278Å channel exhibited the expected behavior: during absence of substorms and visual aurora, intensities less than a few 10's of Raylaighs were observed and had minor or no temporal variations. When subvisual or visual aurora and substorms were present, intense and highly variable emission intensity was observed.

Two similar groups exist in the 4861Å emission data. On quiet days, intense emission was observed early in the evening (2000LT) which fell off as magnetic midnight approached. The cause of this anomalously high emission intensity has not been determined as yet. Disturbed day behavior shows expected relatively low emission intensity in early evening with an emission peak at sometime during the observing period.

Because of low intensity and relatively poorer time coverage in the 5875Å channel, the 5875Å intensity cannot be readily characterized by any identifiable variation in local time on the basis of single day's data, as may be seen in figure 14c.

Insofar as substorm related precipitation and acceleration mechanisms might be expected to affect populations of protons and alpha particles similarly, the data was organized according to substorm time. The reference zero time for this procedure was selected as the time of rapid onset of a magnetic bay on either the Poker Flat or the Fort Yukon magnetograms. In this process we have attempted to select the "obvious" onset time rather than attempt to orient the data towards a more subjective estimate of a slow onset or growth phase. The times and magnitudes of the substorms thus selected are summarized in Table VII.

A distinctive substorm time related intensity pattern shows up in both Hβ 4861Å emission intensity and in the 5875Å channel's intensity as illustrated in figures 15 and 16. Although admittedly a limited data sample, the intensity peaks in both 5875Å and 4861Å channels are better ordered in substorm time than in local time and neither emission shows

Table VII

OCCURRENCES OF MAGNETIC BAYS DURING EXPERIMENT PERIOD

Date (UT)	Poker Flats		Ft. Yukon	
	Onset Time (UT)	Magnitude ΔH_x	Onset Time (UT)	Magnitude ΔH_x
8 March	~ 1600	> -3000 γ	1530	- 850 γ
9 March	0930	~ -2500 γ	1000	- 400 γ
	1036			
	1310	-2500 γ	1300	- 450 γ
11 March	0630	+ 850 γ	0600	+ ~ 100 γ
14 March	0840	- 500 γ	0840	- 150 γ
15 March	1030	- 350 γ	1030	- 300 γ
	1140	- 600 γ	1140	- 300 γ

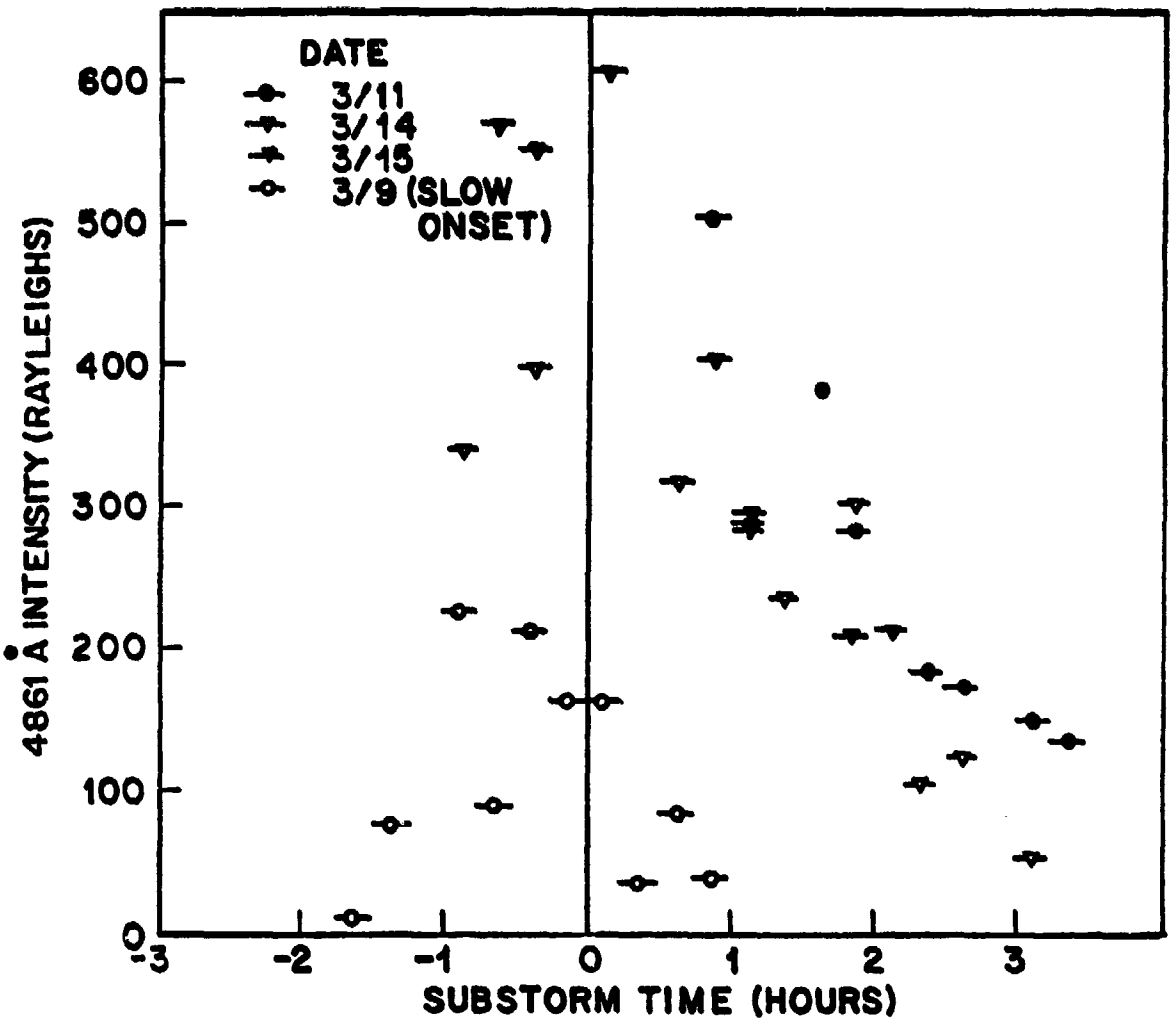

Figure 15 Variations in observed 4861Å, Hβ emission intensity vs. substorm time.

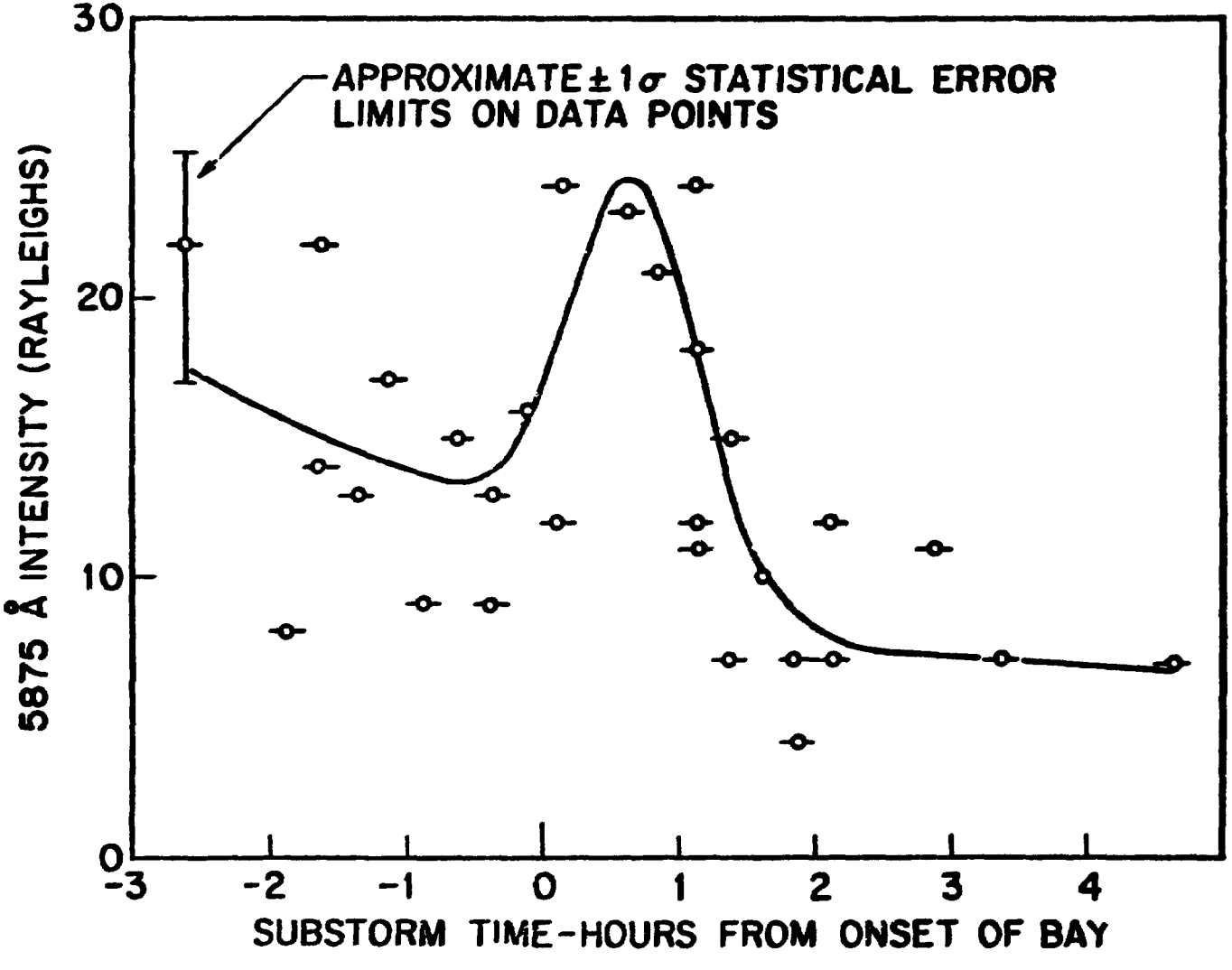

Figure 16 Variations in observed 5875Å emission intensity vs. substorm time.

an equivalent temporal behavior during the two quiet days monitored, hence, the morphology reasonably may be attributed to the substorm phenomena. Other data on substorm related 4861Å emission (see for example, Montbriand, ref. 14) also supports this view point.

It is clear that the substorm related temporal morphology of 4861Å and 5875Å emissions are insufficient to identify He emission. Therefore, a more extensive study of the emission ratios, R_1 = I(4278)/I(5875) and R_2= I(4861)/(5875) and their temporal variations was undertaken.

First, the overall intensity ratio was computed from both quiet and disturbed day data. A mass plot of 4278Å vs. 5875Å intensities and the best linear fit to the zenith data are illustrated in figure 17. The average ratio value R=20 provides a reasonable fit to all of the zenith data; however local time variations in this ratio value exist, as illustrated in figure 18. During two magnetically disturbed periods, the ratio R deviates substantially from the average value 20; however, the ratio increases rather than decreases, which would be the expected deviation if a significant alpha particle precipitation event has occurred.

Similarly, the ratio, R_2 = I(4861Å)/I(5875Å) was computed and examined for anomalous temporal behavior. In this case, inclusion of data from meridional scans in ratio determination produced no consistent ratio value, whereas taking near zenith data only resulted in a ratio value of about 20. Mass plots of 4861Å vs. 5875Å intensities for this case are illustrated in figure 19. Temporal variations on the R_2 value were studied, and indicated some possibility of time dependence during disturbed conditions; however, the data sample intervals and statistical variations on the data preclude any firm conclusion of such an effect. No indications of anomalously low ratio values, which might be indicative of He precipitation increases relative to proton precipitation were found.

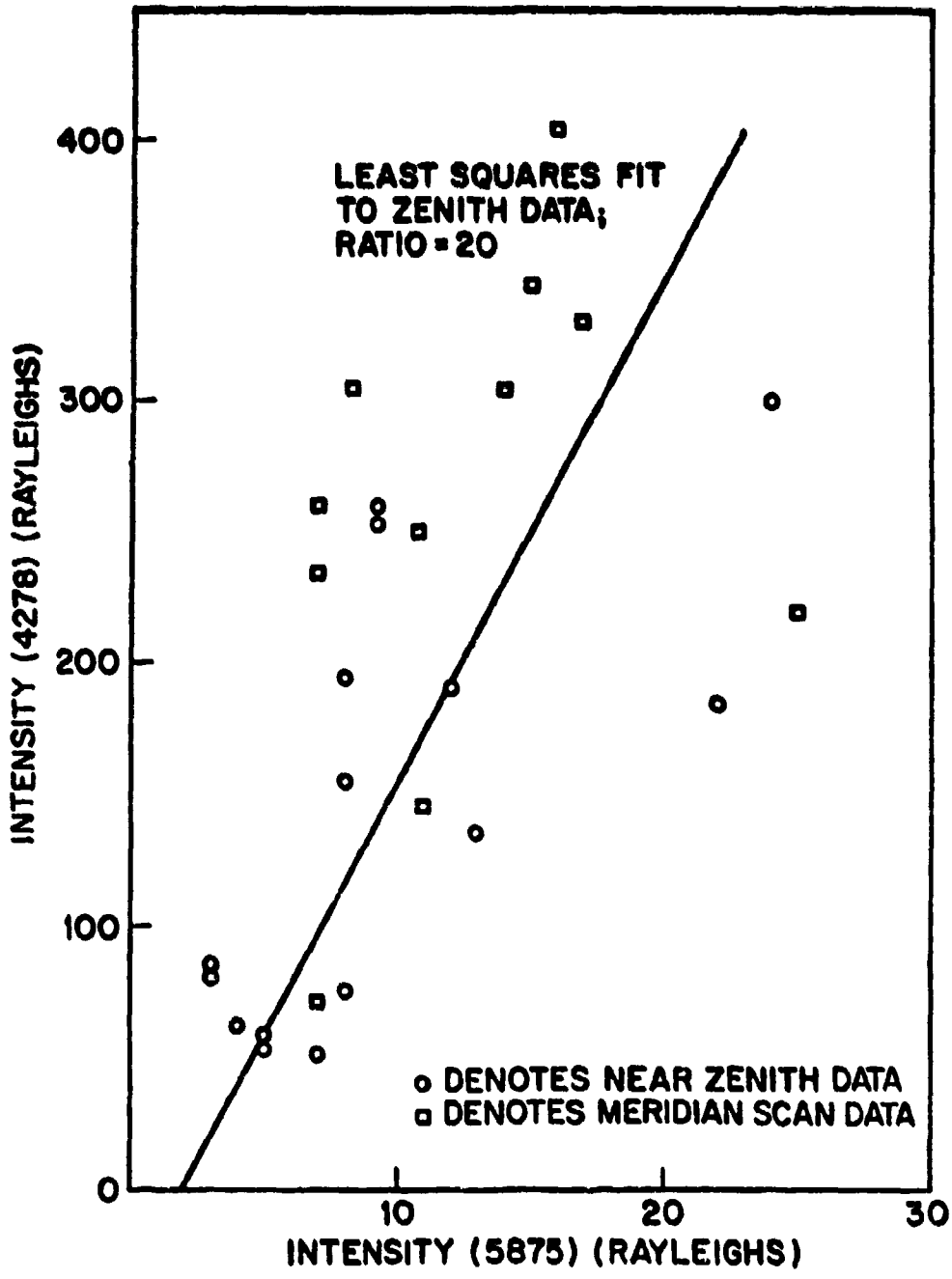

Figure 17 Intensity of 4278Å, N_2^+ 1st negative band emission vs. concurrent intensity of 5875Å emission (N_2 1P and O_2^+ 1N bands).

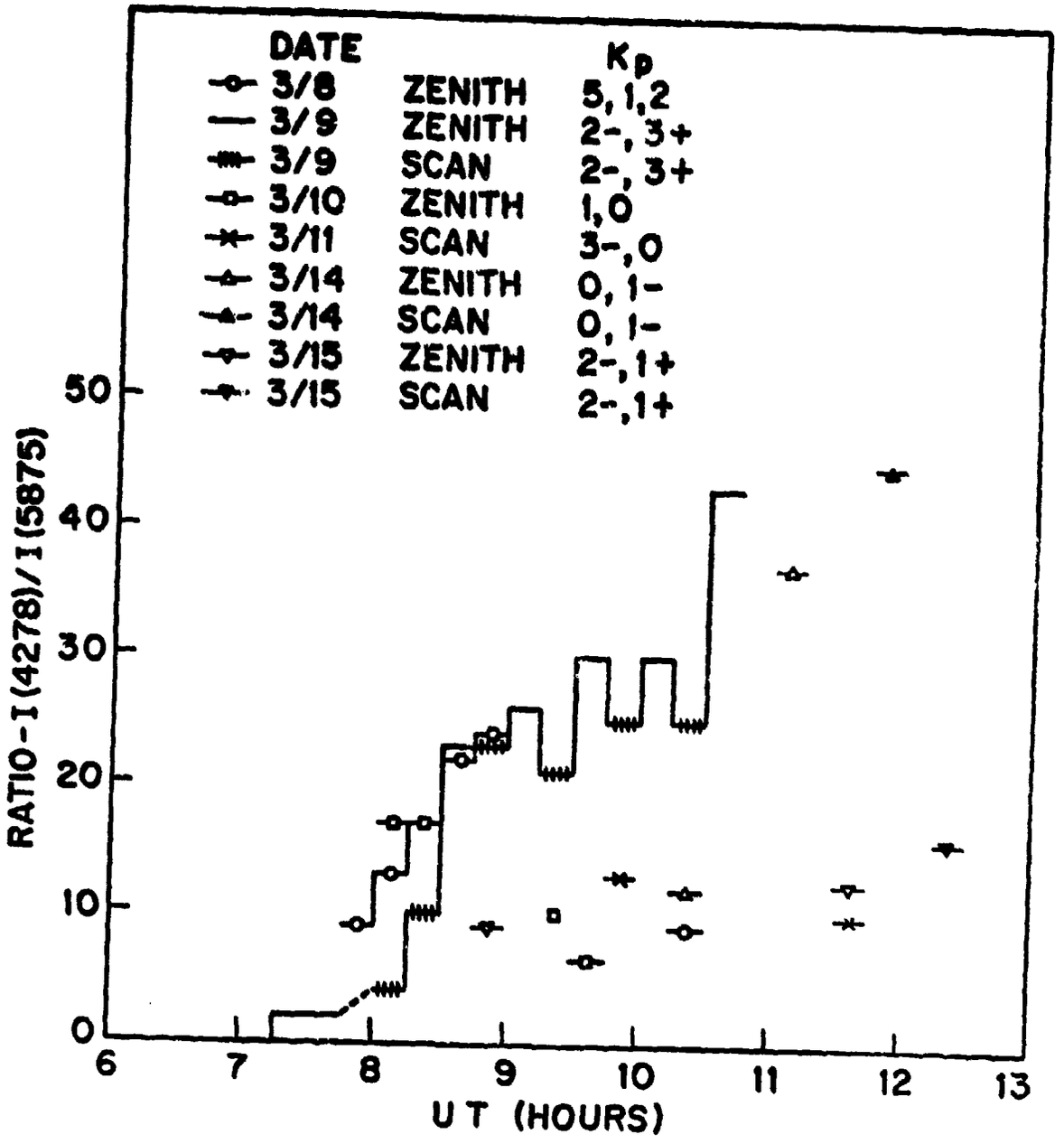

Figure 18 Temporal variation of intensity ratio R.

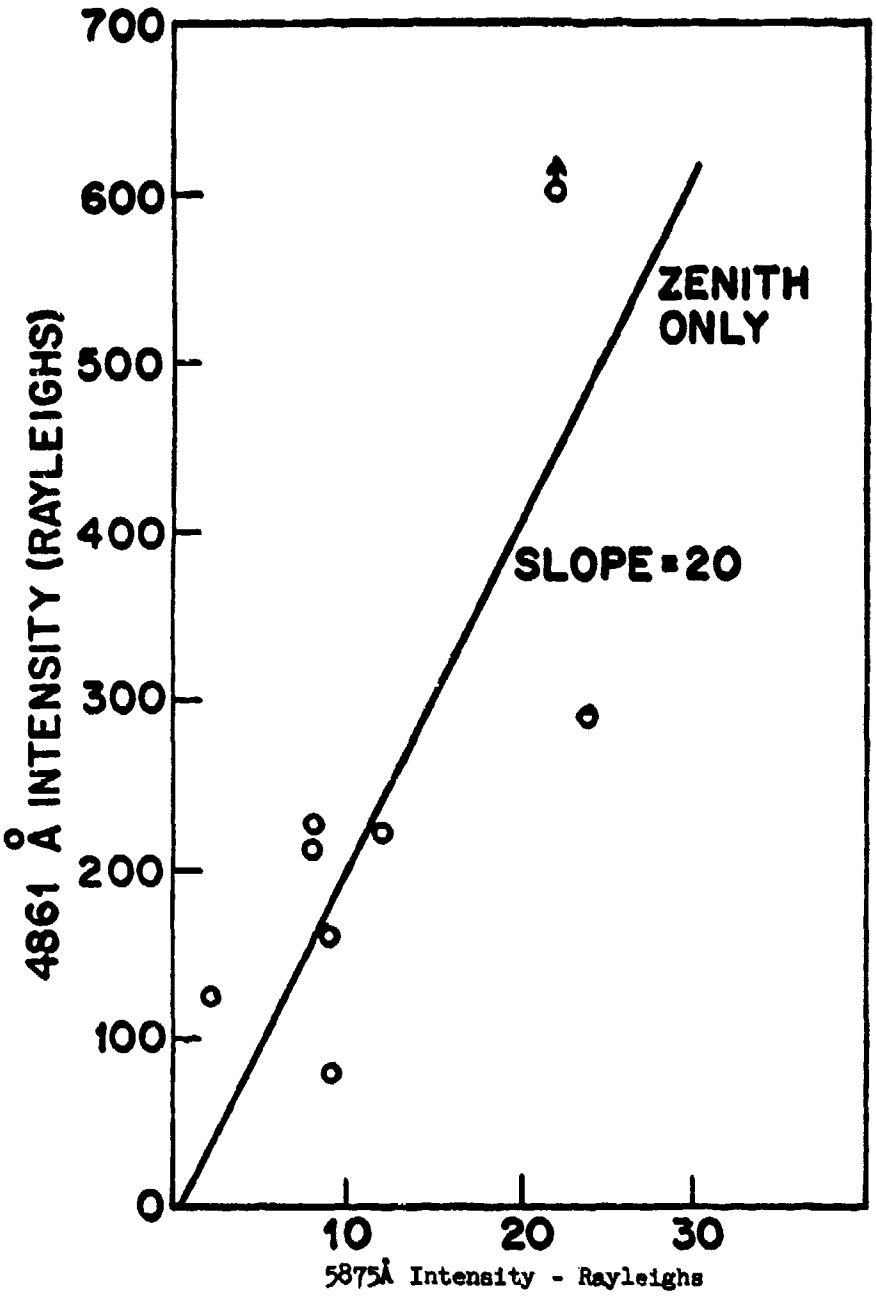

Figure 19 Plot of 4861Å Hβ emission intensity vs. 5875Å intensity for zenith data.

It should be noted at this point, that although the data reported heretofore are concerned with 15 minute averages, a careful survey was made for short period variations such as reported for He emission by Stoffregen (9). For a number of 15 minute intervals cross spectral analyses (see for example Paulson and Shepard, ref. 15) are carried out between 4278 and 5875Å emission intensities in order to determine if any significant short period intensity peaks, or correlated emissions were observed. Of all cases studied, only one 5875Å emission peak (about 10% above background average emission) was detected which could not be reasonably explained by ordinary electron and/or proton auroral fluctuations. Hence, the average intensities reported herein are very closely representative to the actual 5875Å intensities and do not conceal short term activity or intense occasional spikes except as already evidenced in 4278Å auroral emissions.

In addition to measurements of intensities at near zenith orientation, meridional scans were conducted. These scans were analyzed for variations in the 4278/5875Å intensity ratios as well as for evidence for Van Rhyne effect in either emission. Several conditions were observed; in cases where auroral arcs were visible to the north of zenith, some variation in ratio was observed but little significant Van Rhyne effect occurred in either emission. During periods of very low to low subvisual activity wherein a fairly uniform latitudinal distribution of precipitation appeared to be present, slight Van Rhyne effects were observed on both emissions, but the difference between Van Rhyne effect and atmospheric extinction effects which could have compensatory variations could not be determined. Very few cases were observed where Van Rhyne effect was definitely present in 5875Å intensity but not in 4278Å. From these observations, we conclude that the airglow and atmospheric continuum contamination to either 4278Å or 5875Å intensity observations is low.

To summarize, the pertinent and new observations in 4278, 4861 and 5875Å wavelength regions show:

- No discernable local time variation in 5875Å intensity,
- indication of peak 5875Å emission, just after substorm zero time concurrent with a 4861Å intensity peak,
- average intensity ratio R_1 = I(4278)/I(5875) 20 with increasing value during disturbed periods,
- relatively constant intensity ratio, R_2 = I(4861)/I(5875) ~ 20,
- no clear-cut indication of strong OH contamination to the 5875Å intensity data as deduced from Van Rhyne effect analyses.

DISCUSSION

As Omholt (6) and Rather (16) have pointed out, a number of spurious emission features confuse identification of He emissions in the 5875Å spectral region. In particular, a strong feature in the N_2 1PG(9-5) band, two strong spectral lines in the O_2^+ 1N(2-2) band, and two lines of the OH (8-2) band are located in the passband of the filters used herein.

Rather (16) showed through detection of a distinct Van Rhyne effect that OH emission in the R_1 and R_2, K" = 5 lines at 5874.2Å and 5874.3Å, as well as other lines nearby at 5882.7Å and 5882.4Å (K" = 6) could contribute significant emission to a He, 5875Å broadband filter photometer measurement. Of these emission features, the K" = 5 lines lie within our spectral bandpass. Utilizing Chamberlain's (17) estimate of 100 R for the entire OH (8-2) band, and the branching ratios listed therein, we estimate an intensity of about 6 R for these four lines. Van Rhyne effect would contribute a maximum of about 12 R at our maximum zenith angle of 60°. It is possible that the residual 5875Å emission intensity computed in the least squares fit of the value of R intensity ratios is attributable to this emission feature. In addition, it is unlikely that the OH emission would be directly proportional to the incoming particle energy flux as measured by 4278Å intensity.

Molecular emissions excited during electron auroras exhibit approximately constant intensity ratios to the 4278Å or other N_2^+ 1st negative bands, as summarized by Vallance Jones (18). IBC III intensities for the N_2^+(0-1)1N band at 4278Å, N_2(9-5)1P at 5906Å, and O_2^+(2-2)1N band at 5901Å are reported as 16.3 kR, 1.3 kR, and 1.8 kR respectively, thus the ratio R_1 = I(4278)/I(5875) should be approximately 5.2 if the total emission from the N_2 and O_2^+ bands are included. Insofar as the spectral passband of the photometer used included only several strong lines of the bands cited above, the measured ratio R_1 = 20 is entirely consistent with the molecular emission source hypothesis. The distribution of 15 minute ratio values also supports this hypothesis.

The temporal variations of 5875 and 4861Å intensities, however, suggest the possibility of concurrent He and H precipitation. In a search for auroral He line emissions, Eather (19) set an upper limit of the ratio R_2^{-1} of about 0.02 for normal proton precipitation levels and an assumed proton/alpha ratio of 16. For a strong solar storm, the ratio was predicted to be 0.003 or less. Corresponding ratio values computed from the data reported herein are about 0.05, significantly higher than Eather's value. In order to eliminate the necessity for applying variable and somewhat arbitrary corrections for atmospheric extinction vs. zenith angle, only near zenith data were used to compute this value. The relative constancy of the measured ratios R_1 and R_2 and the apparent lack of a strong temporal variation in favor of He emissions suggest that if He precipitation is actually observed in the present data it is a relatively smoothly varying component just as the 4861Å intensity data suggests for proton precipitation. As described in the previous section, explicit absence of strong sporadic emission features in either 4861 or 5875Å spectral regions also indicates that if He emission is present, its temporal variations are not similar to those reported by Stoffregen.

In order to test further the tentative hypothesis that the substorm related 5875Å emission is actually due to alpha particle precipitation, satellite data from STP 71-2 was examined. On the closest passes of this satellite to the Poker Flat, Alaska ground site (in time and longitude for 65° Invariant Geomagnetic Latitude), Shelley (private communication) reported no detectable alpha particle precipitation within the detection capability of the instrument which was 10^5 particles/cm^2 sec ster keV for energies below 12 keV. For this particular energy range, the number of emitted photons per incident alpha was estimated, following the procedure outlined by Eather (20), to be about 0.2 to 0.4. Thus, the satellite detector sensitivity corresponds to an emission intensity of about 0.4 to 3 Rayleighs.

This value is far below that measured, providing direct evidence that if the observed 5875Å emissions are to be attributed to He, then alpha particle precipitation should have been observed in the satellite data.

CONCLUSIONS

Observations of 4278, 4861, and 5875Å emission intensities show that excitation of N_2 and O_2^+ bands in the spectral region of the 5875Å line emission exhibits time varying and substorm related behavior which may serve to effectively mask detection of He emissions by fixed pass-band photometric techniques. Observations of the emission ratios $R_1 = I(4278)/I(5875)$ and $R_2 = I(4861)/I(5875)$ show that the 5875Å band emission is excited with approximately equal efficiency by precipitating protons and electrons. The substorm time-related peak in 4861Å emission is qualitatively different from its temporal variations during quiet times and indicates a different proton precipitation phenomenology than that which exists in the quiet day proton arc. The facility for substorm time organization of this rather limited data sample further confirms the utility of substorm time as an ordering variable as suggested by Eather and Mende (12).

Substorm time related behavior of precipitating particles is of particular importance to ICE CAP in that not only is the onset time of a substorm a real time measurable quantity on the ground, but the particle flux and energy increases now may be more predictable than previously was possible.

In addition to the enhanced possibilities of real time control of rocket launched experiments, the changes in the intensity ratio I(4278Å)/I(5875Å) implies a time variation in particle energy distribution or in excited state population of N_2 and O_2^+ or both. The latter circumstance could be the result of the former. In either case, the ultimate energy sources for infrared active species may be affected as the relative excitation labels of O_2^+, N_2, and other species are changed.

IV. CONCLUSIONS AND RECOMMENDED FUTURE WORK

In this report we have shown that photometric data obtained in Alaska in 1972 and 1973 contributes valuable input to a number of DNA, HAES program goals:

- o Energy input from particle precipitation for the 1972-73 ICE CAP program.
- o Substorm related behavior of electron and proton precipitation, and effects upon atmospheric excited species.
- o Coordinated radar-photometer methods for deriving E-region recombination rates.
- o Coordinated radar photometer methods for estimating importance of transport of ionized and excited species.
- o Estimation of F-region ionized structure and their radar effects from airglow structure maps.

A number of these investigations are continuing in order to provide more quantitative and more precise techniques for measurements of ionospheric drifts and irregularities by coordinated ground based measurements.

Future effort on this aspect of the HAES program should emphasize coordinated measurements between different ground-based instrumentation and rocket and satellite borne sensors. For example, coordinated measurements utilizing the ITS/DNA partial reflection sounder and photometric instrumentation will allow extension of recombination studies from the E-region into the D-region. Likewise, correlation of ground-based photometric measurements of airglow and auroral emissions in different ionospheric layers with clutter radar data will allow better definition of the ionospheric mechanisms which produce clutter; hence, will contribute to better modeling of nuclear burst-produced radar clutter. Previous efforts to coordinate ionospheric scintillation measurements at Goose Bay with photometric F-region structure measurements (described in reference 3) should be resumed.

In summary, as a result of work reported herein, it has become increasingly clear that obtaining the ionospheric data base required by the High Altitude Effects Simulation (HAES) program will involve utilization of several ground-based and rocket or satellite borne instrumentation in closely coordinated experiments. Hence, future effort in the HAES area should emphasize such coordinated experiments involving the photometric, electromagnetic propagation, and in-situ ionospheric measurement techniques.

REFERENCES

1. R.D. Sears, "Coordinated measurements of ionospheric irregularities: Digital photometer design and development," Topical Report DNA 2997T (LMSC D311213), October 20, 1973.

2. R.D. Sears, "Defintion of energy input: Operation ICE CAP," Final Report DNA 2985F (LMSC D311131), Oct. 1, 1972.

3. R.D. Sears, "Goose ionospheric observatory: Photometric measurements program, report of first year operations," Final Report DNA 3033F (LMSC D350544), Nov. 27, 1972.

4. M. Baron, et al., "DNA project 617 radar auroral ionosphere measurements," DNA 3023F, Dec. 1972.

5. A. Brekke and K. Henriksen, Planet. Space Sci., 20, 53-60, 1972.

6. A. Omholt, The Optical Aurora, Springer Verlag, New York, 1971.

7. D. Barbier, Annals Geophys. 17, 3, 1961.

8. D. Barbier, F.E. Roach and W.R. Steiger, J. Res. NBS-D, Radio Propagation 66D, 145, 1962.

9. W. Stoffregen, Planetary Space Sci., 17, 1927, 1969.

10. D.L. Reasoner, Revs. Geophys. and Space Physics, 11, 169, 1973.

11. R.H. Eather and S.B. Mende, in The Radiating Atmosphere, 255-266, D. Reidel Publ. Co., Dordrecht, Holland, 1971.

12. R.H. Eather and S.B. Mende, in publication, J. Geophys. Res., 1973.

13. R.D. Sears, Applied Optics, 12, 1349, 1973.

14. L.E. Montbriand, The Radiating Atmosphere, p. 366-373, D. Reidel Publ. Co., Dordrecht, Holland.

15. K.V. Paulson and G.G. Shepard, J. Atmosph. Terr. Phys., 27, 831, 1965.

16. R.H. Eather, Revs. Geophysics and Space Physics, 11, 155, 1973.

17. J.W. Chamberlain, Physics of the Aurora and Airglow, Academic Press, New York, 1961.

18. A. Vallance-Jones, Space Science Reviews, 11, 776-826, 1971.

19. R.H. Eather, Space Research VIII, 201, North Holland Publ. Co., Amsterdam, and Ann. Geophys., 24, 525, 1968.

20. R.H. Eather, J. Geophys. Res., 71, 4133, 1966.

APPENDIX 1

DATA SYNOPSIS SHEETS

SYNOPSIS OF DATA

Tape: Alaska V-1

Date: 3/20/73 **Time:** 0910 to 1115 UT

Photometer(s): 3c only

General Activity:

0910 to 0925	Very active
0930 to	Weak, widespread activity

Operating Modes:

3c	Time	Mode
	0910 to 0925	N-S scans (160°- 20°)
	0925 to 1115	Z_{mag}

Notes:

1) Records 7 through 9 have meridian scans through intense arcs I_{5577} ~ 100 kR
2) Weak activity at Z_{mag} shows some 4278-5577 and 6300 correlation - fairly low S/N - better after rec # 20 or so/also rec #29 and 30 6300 may have some wavelike structure - 5577 shows fairly good temporal fluctuations.

SYNOPSIS OF DATA

Tape: Alaska V-2

Date: 3.21.73 Time: 0530 to 1310

Photometers: 3b, 3c

General Activity:

0600 - 1300 Intense active auroras, many arcs moving N-S and breakups observed.

1300 to end Fast pulsations present.

Weather: Clear

Operating Mode:

3c	Time	Mode
	0532 - 0630	N-S scans, 20° to 160°
	0630 - 0845	Magnetic zenith
	0845 - 1025	at 80°N elevation angle
	1025 - 1310	Magnetic zenith
3b	0713 - 0818	6300Å
	0818 - 1310	5577Å

Notes:

1) 3b dome frosted up intermittently. Data may be doubtful.

2) Rocket PT (Quiet OH) launched 1011 UT

SYNOPSIS OF DATA

Tape: Alaska VI-1

Date: 3.22.73 **Time:** 0550 - 1250 UT

Photometers: 3b and 3c

General Activity:

0550 - 1100 Weak to moderate activity

1225 UT Fast varying forms

Weather:

Operating Mode:

Operating Mode:

3c	Time	Mode
	0550 - 0610	N-S scans 20° to 160°
	0610 - 0830	Magnetic zenith
	0830 - 1020	80°N elevation angle
	1020 - 1208	Magnetic zenith
	1208 - 1226	80°N elevation angle
	1226 - 1250	Magnetic zenith
3b	0550 - 1226	5577Å
	1226 - 1250	6300Å

Notes:

1) Rocket BB (LWIR-CVF) launched 1213 UT

SYNOPSIS OF DATA

Tape: Alaska VI-2

Date: 3/23/73 **Time:** 0606 - 1340

Photometers: 3b and 3c

General Activity: moderate at times

Weather: Clear

Operating Modes:

	Time	Mode
3c	0606 - 0711	scans 20 - 160°
	0711 - 0903	on 111°N angle
	0903 - 1001	Z_{mag}
	1001 - 1033	111° N angle
	1033 - 1150	120°N angle
	1150 - 1340	131°N angle - N-S switches
3b	0606 - 0726	6300Å
	0726 - 0812	5577Å
	0825 - 1330	5577Å
	1330 - 1340	6300Å

Notes:

1)	Rec 33	Red activity
2)	38	Good S to N motion 3b
3)	35, 36 and 40	Good structure in 3b and 3c
4)	46 - 48	Wavelike in 3b and 3c - aurora?
5)	57, 58	Wavelike in 3b
6)	62 - 65	Structure in 3b - Auroras in ?
7)	82	S to N motion on 3b
8)	84	Can see N-S Red Assymetry 3c
9)	86	10 sec wavelike pulsations 3b
10)	88	Long wavelike S to N 3b
11)	~75 to 92	Structure on 3b, green waves (?)

SYNOPSIS OF DATA

Tape: Alaska VII-1

Date: 3.24.73 Time: 0645 - 1055 UT

Photometers: 3b, 3c

General Activity: Intermittent and moderate

Weather: Thin to thick clouds

Operating Mode:

	Time	Mode
3c	0645 - 1025	scans (20° - 160°)
	1025 - 1042	101° N limit L
	1042 - 1055	Z_{mag}
3b	0645 - 1045	6300Å
	1045 - 1055	5577Å

Notes:

1) Clouds will introduce calibration error for rocket data

2) Records 48 - 54 Activity present

Record 52 at launch - aurora or lights from booster

- 3b doesn't see.

SYNOPSIS OF DATA

Tape: Alaska VII - 2

Date: 3/25/73 Time: 0715 - 1000 UT

Photometers: 3b, 3c

General Activity: Moderate throughout

Weather: Clear

Operating Modes:

	Time	Mode
3c	0715 - 0755	at indeterminant elevation angle
	0755 - 1000	at 131°N (49° el L)
3b	0715 - 1000	5577Å

Notes:

1) Records 12 - 21 Good! on 3b str.

2) 26 Good structure in 3b and auroras in 3c

3) 27 Aurora - 3c and 3b effects also

4) Records 33-34 Aurora in FOV - 3c

5) Records 36-39 Aurora in FOV - 3b. structure and drift

SYNOPSIS OF DATA

Tape: Alaska VIII-1

Date: 3.26.73 Time: 0700 to 1050 UT

Photometers: 3b, 3c

General Activity:

0700 - on: Strong activity in north - partially obscured by clouds and haze. Good red structure observed on TV.

Weather: hazy and cloudy

Operating Modes:

3c	Time	Mode
	0700 - 0851	Magnetic zenith
	0851 - 1050	80°N elevation angle
3b	0700 - 0825	5890Å
	0825 - 1050	6300Å

Notes:

1) Rockets BB and PT launched at 0937:46 and 0938:26 UT.

2) Haze conditions may preclude accurate intensity calibrations.

SYNOPSIS OF DATA

Tape: Alaska VIII-2

Date: 3/27/73 **Time:** 0610 - 1330 UT

Photometers: 3b and 3c

General Activity:

Weather: Clear

Operating Modes:

3c	Time	Mode
	0610 - 0809	$Z_{magnetic}$
	0809 - 0927	101° N angle (79° el angle)
	0927 - 0929	$Z_{magnetic}$
	0929 - 0950	101° N angle
	0950 - 1330	$Z_{magnetic}$
3b	0610 - 0857	6300Å
	0857 - 1000	5577Å
	1009 - 1213	5890Å
	1213 - 1330	5577Å

Notes:

1)	Records 46-48 on	large structure in 3b - break at zenith
2)	53	intense activity during and preceding launches
3)	55	3b structure
4)	56	~ 50 kR arc with red enhancement
5)	57	~ 100 kR arc passed - red correlation possibly Na correlation on 3b
6)	62-66	low level activity

SYNOPSIS OF DATA

Tape: Alaska IX-1

Date: 3/28/73 Time: 0715 - 1200 UT

Photometers: 3b and 3c

General Activity: Arcs to North
Weak pulsating activity later in night

Weather: Clear to slight haze later

Operating Modes:

	Time	Mode
3c	0715 - 0725	Z_{mag}
	0725 - 0727	scan 20° - 160°
	0727 - 0830(est)	stuck at S limit of 20°
	0830 - 0842	scans
	0842 - 1200	Z_{mag}
3b	0715 - 0844	5577Å
	0844 - 1115	5890Å
	1115 - 1200	5577Å

Notes:

1) Records 25 - 27 Good Green - Red Correlation on scans/also structure in 3b

33 Weak green activity

34 Has strong R-G correlation - weak arc?

2) Rec 59 3c may have good decay times for red and green shows good 3b and 3c pulsation (arc going through?)

3) Rec 27 To end shows structured 3b features and weak pulsating 4278 background

SYNOPSIS OF DATA

Tape: Alaska IX -II

Date: 3/29/73 Time: 0800 to 1245 UT

Photometers: 3c and 3b

General Activity: Low

Weather: Thin clouds or haze after about 0930

Operating Modes:

	Time	Mode
3c	0800 - 0840	Z_{mag}
	0840 - 0925	101° N (79° el L)
	0925 - 1051	Z_{mag}
	1000 - 1010	DCR run
	1051 - 1245	N-S scans 20° - 160°
	Note: RT data ends at 1225	
3b	0800 - 0925	5577Å
	0925 - 1050	Na 5890Å
	1050 - 1245	5577Å

Notes:

1) Records 20-23 show low level 3c activity - also some wavelike (?) structure on 3b, 0843 on

SYNOPSIS OF DATA

Tape: Alaska XI-1

Date: 4/1/73 Time: 0745 - 1230 UT

Time correction: Add 69 sec to get UT (true)

Photometers: 3b and 3c (4278, 5577 only)

General Activity: Moderately high all night - several arcs and several breakups observed

Weather: Clear

Operating Modes:

3c	Time	Mo	Mode
	0745 - 1230		Z_{mag}
3b	0745 - 0820		6300Å
	0820 - 0925		5577Å
	0925 - 1230		6300°

Notes:

1) Records 18-20 Shorter term variable activity

2) Record 26 Arc in FOV - N/S drift measurable

3) Records 25-30 Strong activity - arcs

4) Records 30-50 low level - slowly varying activity

5) Records 49-53 shorter term variations ~ 5 sec

6) Records 53-60 large scale - long term variations

SYNOPSIS OF DATA

Tape: Alaska XI-II

Date: 4/2/73 Time: 0730 - 1155

Photometers: 3c (4278, 5577 only) and 3b

General Activity: Very high - many breakups - morning sector pulsating forms

Weather: Clear

Operating Modes:

3c	Time	Mode
	0730 - 1155	Z_{mag}
	1055 - 1155	Z_{mag} - fast (0.2 sec) mode
3b	0730 - 0930	6300Å (noisey data)
	0930 - 1155	5577Å

Notes:

1) Records 30-41 Rec 34 very good !!
Very high Grn and Blue activity at Z_{mag} can also get drift vel. on 3b after 0930

2) Rec 47 to end Fast mode has good 3c and 3b pulsation coherency data.

APPENDIX 2

CORRELATION AND POWER SPECTRAL DENSITY PROGRAM

10.8. AUXCOR - Auto-Correlation and Cross-Correlation Analysis

10.8.1. Purpose

To compute the auto- and the cross-correlations of several stationary time series at all required lags.

10.8.2. Calling Sequence

```
CALL AUXCOR(X,N,NSRS,M,IT,COR,XBR,XBRL,S,SL,NMX,NSMX,MMX)
```

where

X	is the array of observations of the time series.
N	is the number of observations in each time series.
NSRS	is the number of time series.
M	is the number of lag terms.
IT	=0, if the series have been detrended; =1, if the series have not been detrended.
COR	is the array of auto-correlations and cross-correlations.
XBR	is the array of means.
XBRL	is the array of lagged means.
S	is the array of sums of squares.
SL	is the array of lagged sums of squares.
NMX	is the maximum number of points per time series as defined by the calling program.
NSMX	is the maximum number of time series as defined by the calling program.
MMX	is the maximum number of lags as defined by the calling program.

10.8.3. Method

The cross-correlation between two series at a given lag value v is:

$$r_{ij}(v)=R_{ij}(v)/(S_{i,o}S_{j,v})^{\frac{1}{2}}$$

where

$R_{ij}(v)$ is the cross-covariance function

$$R_{ij}(v) = \frac{1}{N-v} \sum_{t=1}^{N-v} (X_{t,i}-\bar{X}_{i,o})(X_{t+v,j}-\bar{X}_{j,v})$$

$\bar{X}_{i,o}$ is the mean

$$\bar{X}_{i,o} = \frac{1}{N-v} \sum_{t=1}^{N-v} X_{t,i}$$

$\bar{X}_{j,v}$ is the lagged mean

$$\bar{X}_{j,v} = \frac{1}{N-v} \sum_{t=v+1}^{N} X_{t,j}$$

$S_{i,o}^{\frac{1}{2}}$ is the sum of squares

$$S_{i,o} = \frac{1}{N-v} \sum_{t=1}^{N-v} (X_{t,i}-\bar{X}_{i,o})^2$$

$S_{j,v}^{\frac{1}{2}}$ is the lagged sum of squares

$$S_{j,v} = \frac{1}{N-v} \sum_{t=1}^{N-v} (X_{t+v,j} - \bar{X}_{j,v})^2$$

$r_{ii}(v)$ is the auto-correlation function for the ith time series.

10.9. POWDEN - Power Density Functions

10.9.1. Purpose

To compute the co-spectral and cross-spectral density functions of a set of time series.

10.9.2. Calling Sequence

```
CALL POWDEN(Y,N,NSERS,M,NQ,IT,COR,F,Q,A,PH,COH,G,DEVD,
            NMX,NSMX,MMX,NQMX,XBR,XBRL,S,SL)
```

where

Y	is the array of observations for the time series.
N	is the number of observations in each time series.
NSERS	is the number of time series.
M	is one more than the maximum number of lags for the cross-correlation analysis.
NQ	is the maximum number of periods to be covered in the density calculations.
IT	=0, if the series are detrended; =1, if not.
COR	is the array of auto- and cross-correlations computed.
F	is the array of cross-spectral density estimates.
Q	is the array of quadrature densities.
A	is the array of spectral amplitudes.
PH	is the array of spectral phases.
COH	is the array of spectral coherencies.
G	is the array of spectral gains.
DEVD	is the array of standard errors of the natural logarithms of the co-spectral estimates.
NMX	is the maximum number of correlation lags as specified by the calling program.

NSMX is the maximum number of time series as specified by the calling program.

MMX is the maximum number of correlation lags as specified by the calling program.

NQMX is the maximum number of periods in the spectral density analysis as specified by the calling program.

XBR is the array of lagged means.

S is the array of standard deviations.

SL is the array of lagged sums of squares.

10.9.3. Method

- Let $r_{ij}(v)$ be the cross-correlation between series i and j for lag v. The normalized co-and cross-spectral density function at period p is given by

$$f_{ij}(p)=\frac{1}{2\pi}\left\{r_{ij}(o)+\sum_{v=1}^{m} k\left(\frac{v}{m}\right)\cos\left(\frac{2\pi v}{p}\right)\left[r_{ij}(v)+r_{ji}(v)\right]\right\}$$

where the spectral window k(.) is defined as

$$k(u) = 1-6u^2+u^3 \qquad 0 \le u \le 0.5$$

$$= 2(1-u^3) \qquad 0.5 \le u \le 1$$

$$= 0 \qquad u \ge 1$$

- The quadrature spectrum is defined by

$$q_{ij}(p) = \frac{1}{2\pi}\sum_{v=1}^{m} \sin\left(\frac{2\pi v}{p}\right) k\left(\frac{v}{m}\right)\left[r_{ij}(v)-r_{ji}(v)\right]$$

- The other spectral quantities computed are

Amplitude: $A_{ij}(p) = \left\{f_{ij}^2(p) + q_{ij}^2(p)\right\}^{\frac{1}{2}}$

Phase: $PH_{ij}(p) = \tan^{-1}\left[(q_{ij}(p)/f_{ij}(p)\right]$

Coherence: $C_{ij}(p) = f_{ij}(p)/(f_{ii}(p)f_{jj}(p))$

Gain: $G_{ij}(p) = A_{ij}(p)/f_{jj}(p)$

- The standard error of the natural logarithm of the estimate of the co-spectral density at period p for series i is defined as

$$d_i(p) = (0.54m/n)^{\frac{1}{2}} f_{ii}(p) \qquad I < p < NQ$$

$$= (1.08m/n)^{\frac{1}{2}} f_{ii}(p) \qquad p=0 \text{ or } p=NQ$$